Draft version March 13, 2022
Typeset using LaTeX **twocolumn** style in AASTeX62

arXiv:1711.05964v2 [astro-ph.SR] 16 Aug 2018

New Neutron-Capture Site in Massive Pop III and Pop II Stars as a Source for Heavy Elements in the Early Galaxy

Projjwal Banerjee,[1] Yong-Zhong Qian,[2,3] and Alexander Heger[4,3]

[1] *Department of Astronomy, School of Physics and Astronomy, Shanghai Jiao Tong University, Shanghai 200240, China*
[2] *School of Physics and Astronomy, University of Minnesota, Minneapolis, MN 55455*
[3] *Tsung-Dao Lee Institute, Shanghai 200240, China*
[4] *Monash Centre for Astrophysics, School of Physics and Astronomy, Monash University, Vic 3800, Australia*

(Dated: March 13, 2022)

ABSTRACT

We propose a new neutron-capture site in early metal-poor and metal-free stars of ~ 20–$30\,M_\odot$ that results from proton ingestion in the He shell during late stages of the stars' lives. Most of the neutron capture occurs in the first $\lesssim 10^6$ s following proton ingestion when $^{13}C(\alpha,n)^{16}O$ produces neutron densities typical of the intermediate neutron-capture process. This phase may be followed by another lasting $\gtrsim 10^7$ s with $^{17}O(\alpha,n)^{20}Ne$ producing much lower neutron densities typical of the slow neutron-capture process. We explore the dependence of the proposed neutron-capture nucleosynthesis on the amount and time of proton ingestion, the initial metallicity, and the ensuing supernova shock. We obtain a range of heavy element abundance patterns including those attributed to the slow neutron-capture process or a combination of the slow and rapid neutron-capture processes. Our results can account for the observed ubiquity of heavy elements such as Sr and Ba in the early Galaxy and explain puzzling abundance patterns of these elements in at least some very metal-poor (VMP) stars including those of the carbon-enhanced varieties. In the latter case, the explanation by the single site proposed here differs from the existing paradigm that attributes various classes of VMP stars to enrichment by multiple different sites.

1. INTRODUCTION

Massive stars of $\gtrsim 8\,M_\odot$ have lifetimes of ~ 10 Myr and die as core-collapse supernovae (CCSNe). They are the predominant source for chemical enrichment of the interstellar medium (ISM) during the first ~ 1 Gyr after the Big Bang. Very metal-poor (VMP) low-mass stars formed at those early times have typical Fe abundances less than about one-hundredth the solar value ($[Fe/H] \equiv \log(Fe/H) - \log(Fe/H)_\odot \lesssim -2$). They live until today and are fossil records of the early ISM. Elements heavier than the Fe group like Sr (mass number $A \sim 88$) and Ba ($A \sim 135$–138), whose solar abundances were mainly produced by the slow (s) and rapid (r) neutron-capture processes, have been observed in the majority of VMP stars (Roederer 2013). Moreover, measurements of multiple heavy elements in individual stars have revealed diverse abundance patterns encompassing those characteristic of the r or s process, and those in between for the so-called r/s stars (Beers & Christlieb 2005). The ubiquity of heavy elements and the diversity of their patterns in VMP stars, however, are difficult to explain in the existing framework. Regular CCSNe can only produce elements up to $A \lesssim 120$ in the neutrino-driven wind (Roberts et al. 2010; Arcones & Thielemann 2013), and therefore, can only account for the presence of Sr but not the ubiquity of heavier elements like Ba. Although rare events associated with massive stars, such as jet-induced CCSNe (Winteler et al. 2012) or neutron star mergers (Lattimer & Schramm 1974; Eichler et al. 1989; Freiburghaus et al. 1999), can produce Ba by the r-process, they are too infrequent to have provided pervasive enrichment to the ISM and cannot explain patterns sharply different from the r-process kind. This is consistent with only ~ 3–$5\,\%$ of the VMP stars having strong r-process enrichment (Roederer et al. 2014a).

Particularly puzzling are the carbon enhanced metal-poor (CEMP) stars with $[C/Fe] > 0.7$, which are further divided into three groups depending on their heavy element enrichment (Beers & Christlieb 2005). Stars with low levels of heavy elements ($[Ba/Fe] < 0$) are called CEMP-no stars. These are currently thought to have formed from an ISM polluted by massive stars of the

Corresponding author: Projjwal Banerjee
projjwal@sjtu.edu.cn

very first (Pop III) and very early (Pop II) generations. Several models have been put forward for the polluting sources, which include rotating massive stars (Meynet et al. 2006) and CCSNe with low to medium explosion energies. The latter source preferentially ejected C relative to Fe, leading to [C/Fe] > 0.7 (Umeda & Nomoto 2005; Nomoto et al. 2005; Tominaga et al. 2014; Heger & Woosley 2010). The origin of the heavy elements such as Ba in the CEMP-no stars, especially those thought to have been enriched by Pop III sources, remains unclear.

Another subclass of CEMP stars is the so-called CEMP-s stars with s-process-like patterns ([Ba/Eu] $>$ 0.5) and high enrichment of heavy elements ([Ba/Fe] $>$ 1) (Beers & Christlieb 2005). In contrast to CEMP-no stars, these are thought to be the result of surface pollution by binary companions and do not reflect the composition of the ISM from which they were born. Specifically, the primary member of a binary produced the s-process elements during its asymptotic giant branch (AGB) phase and then transferred these elements along with C to the secondary member, which is observed as a CEMP-s star today. This prevailing scenario can explain the abundance patterns of heavy elements in most CEMP-s stars reasonably well, although patterns in some CEMP-s stars remain a challenge for this mechanism (Bisterzo et al. 2012). In addition, whereas most CEMP-s appear to be in binaries (Lucatello et al. 2005) as required by the above binary mass transfer scenario, recent observations indicate that $\sim$ 10–30 % of such stars could be single (Hansen et al. 2016b). Therefore, some other mechanism is required to provide s-process enrichment to single CEMP-s stars. Fast-rotating metal-poor massive stars ("spinstars") have been proposed as another s-process site in the early Galaxy (Pignatari et al. 2008; Frischknecht et al. 2016), but they dominantly produce elements around Sr with some Ba and very little Pb ($A \sim 208$). Therefore, they cannot explain the overall patterns in those CEMP-s stars with substantial Pb abundances.

The so-called CEMP-r/s stars form yet another subclass that shows high enrichment in heavy elements with patterns in between those for the r and s processes ($0 <$ [Ba/Eu] < 0.5). The origin of these stars remains a major puzzle although various scenarios have been proposed (Cohen et al. 2003; Barbuy et al. 2005; Jonsell et al. 2006). In a popular scenario, CEMP-r/s stars have a similar origin to CEMP-s stars in binaries, except that the former stars were born in highly r-process-enriched parent clouds, thereby acquiring their r-like features. Their s-like features were due to binary mass transfer just like the CEMP-s stars. Recent studies, however, have shown that this scenario is disfavored and that most likely a new neutron-capture site produced both the r and s-like features in CEMP-r/s stars (Lugaro et al. 2012). The so-called intermediate (i) process (Cowan & Rose 1977) has been proposed as a possible mechanism. This process operates at neutron densities much higher than those typical of the s-process but lower than those for the r-process. It has been shown that the required i-process neutron densities of up to $\sim 10^{15}\,\mathrm{cm}^{-3}$ can be generated via $^{12}\mathrm{C(p,\gamma)}^{13}\mathrm{N}(e^{+}\nu_e)^{13}\mathrm{C}(\alpha,\mathrm{n})^{16}\mathrm{O}$ following proton ingestion in He layers of low to intermediate mass stars during late stages of their evolution (Fujimoto et al. 2000; Campbell et al. 2010; Herwig et al. 2011; Jones et al. 2016). Transfer of the i-process products along with C to a low mass binary companion would result in the latter being observed as a CEMP-r/s star today. One-zone parametric studies by Dardelet et al. (2014) and more recently by Hampel et al. (2016) have shown that the i-process can produce the abundance patterns of heavy elements in many CEMP-r/s stars very well. Therefore, the leading scenarios for both CEMP-s and CEMP-r/s stars require mass transfer following neutron-capture nucleosynthesis by low to intermediate mass companions in binaries. We note that rapidly accreting white dwarfs were proposed as another site for the i-process (Denissenkov et al. 2017).

Here we report a new site for heavy element synthesis by neutron capture in early massive stars of $\sim$ 20–30 $\mathrm{M}_{\odot}$ with zero (Pop III) to low (Pop II) metallicity ([Fe/H] $\lesssim -2$) at birth. A few years prior to the end of such a star's life, C has been depleted in the center and the He shell becomes convective. Protons are present at low levels in the outer He shell and some of them are ingested into the inner He shell by convective boundary mixing. Further transport to the hotter region initiates the familiar reaction sequence $^{12}\mathrm{C(p,\gamma)}^{13}\mathrm{N}(e^{+}\nu_e)^{13}\mathrm{C}(\alpha,\mathrm{n})^{16}\mathrm{O}$ that produces neutron densities corresponding to both the i-process and the s-process. As a result, elements up to Bi ($A = 209$) are produced. The final abundance pattern can vary from s-like to r/s-like, depending on the amount of proton ingestion and the time available for neutron capture before core collapse. Instances of proton ingestion in the convective He shell have been reported earlier for zero-metallicity stars with similar masses to the above range (Heger & Woosley 2010; Limongi & Chieffi 2012). After we completed the study for this paper, Clarkson et al. (2018) reported work on proton ingestion in the convective He shell in a zero-metallicity 45 $\mathrm{M}_{\odot}$ star, which led to large energy generation and neutron capture. That "i-process", however, produced elements only up to the Fe group. Here we present a detailed analysis of the

neutron-capture nucleosynthesis in Pop III and Pop II stars of $\sim$ 20–30 $M_\odot$, focusing on a 25 $M_\odot$ star with an initial metallicity of zero to $[Z] = -1$. Specifically, we examine the dependence of the nucleosynthesis on the amount and time of proton ingestion, among other things.

The neutron-capture site presented in this study resides in a significant fraction of early massive stars and can explain a number of puzzles:

1. the ubiquity of heavy elements such as Ba in VMP stars, including CEMP-no stars with low enhancement of such elements, some of which are considered as records of nucleosynthesis by the first generation of stars,

2. heavy-element patterns in some CEMP-s stars, including single stars whose enrichment cannot be explained by binary mass transfer,

3. the origin of heavy elements in some CEMP-r/s stars,

4. the origin of stars with heavy-element patterns similar to CEMP-s and CEMP-r/s stars but with much lower enhancement (Spite et al. 2014), and

5. the early onset of s-like signature in VMP stars (Simmerer et al. 2004; Suda et al. 2008).

We discuss our methods of modeling proton ingestion and the associated nucleosynthesis in early massive stars in §2. The results on nucleosynthesis are presented and compared with observations in §3. We discuss the implications of our results for general observations of VMP stars in §4. We summarize and give our outlook in §5.

2. METHODS

We study nucleosynthesis in non-rotating stars of 15–40 $M_\odot$ with an initial metallicity of zero to $[Z] = -2$ (corresponding to [Fe/H] ~ -2). The corresponding initial composition is scaled from the solar abundances for Be to Zn and taken from the results of Big Bang nucleosynthesis for H to Li. The elements above Zn are excluded so that they can be clearly attributed to nucleosynthesis in the star. We use the 1D hydrodynamic code KEPLER (Weaver et al. 1978; Rauscher et al. 2003) to calculate the evolution and associated nucleosynthesis of a star from its birth to its death in a core-collapse supernova (CCSN). In all the models, we find that the base of the He shell becomes convective when the temperature at the center reaches $T \sim 1.2 \times 10^9$ K and most of the C there has been exhausted. This onset of convection occurs a few years before the CCSN as the star shrinks in order to increase the central temperature to burn C. For a 25 $M_\odot$ star, the radius at the base of the He shell decreases by ~ 60 % from C ignition to C depletion at the center. As a result, the temperature at this position increases from 1.75×10^8 K to $\sim 2.7 \times 10^8$ K, causing a large increase in energy production by the triple alpha reaction. The excess energy generated can only be efficiently transported by convection, which is modeled with the standard mixing length theory (MLT) in KEPLER. The convection at the base of the He shell grows until almost the entire He shell becomes fully convective when C is depleted at the center. The structure of a metal-free 25 $M_\odot$ star at this time is shown in Fig. 1, where the convective region is indicated as the gray area.

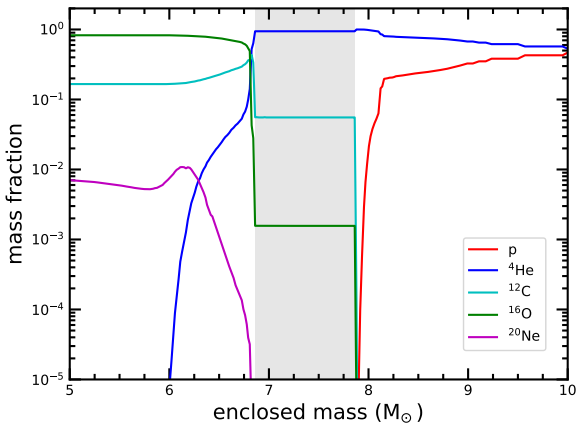

Figure 1. Mass fractions of protons (*red*), ^{4}He (*blue*), ^{12}C (*cyan*), ^{16}O (*green*), and ^{20}Ne (*magenta*) as functions of mass coordinate for a metal-free 25 $M_\odot$ star at central C depletion. The convective He shell is indicated by the grey region.

2.1. *Proton Ingestion in the Convective* He *Shell*

There are $\sim 10^{-3}$–10^{-2} $M_\odot$ of protons with mass fractions of 10^{-5}–10^{-2} in the outer He shell just above the boundary of the convective He shell in a $\sim$ 20–30 $M_\odot$ star. Some of these protons can be ingested in the convective region when convection grows to encompass the corresponding layers or by mixing processes such as overshoot and turbulent entrainment at the convective boundary. The default treatment of overshoot in KEPLER allows a single zone at the boundary to mix slowly when a region becomes unstable to convection by the Ledoux criterion. Only tiny amounts of protons are ingested in a few models with this treatment.

A different overshoot prescription (Herwig 2000) is used in the stellar evolution code MESA (Paxton et al. 2011). In this prescription, regions outside the convective boundary are allowed to mix with an exponentially

decaying diffusion coefficient

$$D_{\rm osht} = D_0 \exp\left(\frac{-2z}{f H_{\rm P}}\right), \quad (1)$$

where D_0 is the diffusion coefficient calculated from the MLT for a zone just inside the convective region, z is the distance of overshoot from the convective boundary, $H_{\rm P}$ is the pressure scale height, and f is a dimensionless parameter controlling the efficiency of overshoot. We modified KEPLER to implement this overshoot prescription for the He shell. A recent study comparing KEPLER and MESA models (Sukhbold & Woosley 2014) found that $f = 0.025$ resulted in similar structure for massive stars. Using this number as the default value of f, we found that $\sim 10^{-5}$–$10^{-4}\,{\rm M}_\odot$ of protons were ingested in $\sim$ 20–30 $\rm M_\odot$ models by the time of central C depletion. For models with $[Z] \lesssim -4$ or $f \gtrsim 0.025$, additional episodes of proton ingestion occur later when the star contracts during the stage from central O depletion to core collapse.

Proton ingestion does not occur in stars of $< 20\,{\rm M}_\odot$, where convection is unable to reach the layers with protons in the outer He shell. On the other hand, the outer He shell in stars of $> 30\,{\rm M}_\odot$ has relatively high temperature and protons there have been burned away by the time the He shell becomes fully convective. So proton ingestion does not occur in such stars, either. Thus, proton ingestion is limited to $\sim$ 20–30 $\rm M_\odot$ stars.

Because 1D models have large uncertainties in treating overshoot specifically and convective boundary mixing in general, we used the above overshoot prescription primarily to estimate the level of proton ingestion that can occur in such models. Proton ingestion found in our 1D study, however, may also be common in 3D simulations. For example, additional mixing due to turbulent entrainment was seen in convective boundary layers in 3D stellar models (Meakin & Arnett 2007).

2.2. *Transport of Ingested Protons in the Convective* He *Shell*

In order to study the nucleosynthesis resulting from proton ingestion in detail, we focus on 25 $\rm M_\odot$ stars with varying initial metallicities. We evolve a star from its birth to the point when its central temperature reaches $T = 1.2 \times 10^9\,{\rm K}$ using the default mixing scheme in KEPLER. Then proton ingestion is simply implemented by injecting an amount $M_{\rm p} = 10^{-6}$–$10^{-3}\,{\rm M}_\odot$ of protons in a single zone at the upper boundary of the convective He shell at central C depletion for most models. Single ingestion at central O depletion and multiple episodes of ingestion are also explored for other models.

Transport of ingested protons in the convective He shell is difficult to model with the standard MLT used in KEPLER and most other 1D stellar evolution codes. In fact, studies of proton ingestion in He layers of post-AGB and super-AGB stars (Herwig et al. 2011; Jones et al. 2016) have shown that the MLT is inadequate. Similarly to these studies, we find that injecting protons at the top of the convection shell leads to a slightly higher entropy for the proton-enriched zone compared to the rest of the shell. For $M_{\rm p} \gtrsim 10^{-5}\,{\rm M}_\odot$, this entropy barrier causes a split in the convective He shell, where bulk of the protons are trapped in the upper convective zone with temperatures of $\lesssim 1.3 \times 10^8\,{\rm K}$. Because of this trapping, only $\lesssim 10^{-5}\,{\rm M}_\odot$ of protons can reach the base of the He shell, where the temperature is high enough to initiate neutron production via the usual reaction sequence $^{12}{\rm C(p,\gamma)^{13}N}(e^+\nu_e)^{13}{\rm C}(\alpha,{\rm n})^{16}{\rm O}$. 3D simulations of AGB and post-AGB stars, however, indicate that such splitting of the convective He shell would likely be delayed (Herwig et al. 2011) or may even be absent (Stancliffe et al. 2011). In either case, protons can travel downwards to hotter regions to initiate neutron production. Clearly, ingestion and transport of protons are intrinsically 3D phenomena and cannot be captured accurately in 1D (Herwig et al. 2014).

For the reasons given above, most previous studies on nucleosynthesis from proton ingestion employed one-zone network calculations using typical temperature, density, and composition from 1D stellar models as input. Here we perform a multi-zone calculation taking advantage of two separate networks incorporated in KEPLER to compute energy generation and nucleosynthesis, respectively. A 19 isotope network, APPROX19, is used for energy generation and stellar structure evolution, whereas a large adaptive post-processing network is used to calculate nucleosynthesis accurately. The latter includes isotopes up to atomic number 85 between the proton and neutron drip lines. The number of isotopes in the network grows to a maximum of $\sim$ 1,400 for neutron-capture nucleosynthesis during pre-CCSN evolution, and to a maximum of $\sim$ 2,100 for explosive nucleosynthesis during shock propagation. The rates adopted in this study are the same as those listed in detail by Rauscher et al. (2002). Table 1 gives the references for the adopted rates for neutron, proton, and α-particle reactions on ^{12,13}C, ^{13,14}N, and ^{16,17}O. These rates are the most relevant for neutron production following proton ingestion. For neutron capture, theoretical rates from Rauscher et al. (2000) are used, supplemented by recommended experimental rates from Bao et al. (2000) whenever available. We note that most of the rates have not been measured in the astrophysically-relevant en-

ergy regime. Whereas efforts to update all the rates are important, changes to the pertinent rates for neutron production and most other rates are expected to be within the current uncertainties and would not qualitatively alter our results.

To avoid the issues related to splitting of the convective zone mentioned above, we model the ingestion of protons using only the post-processing network without changing the composition in APPROX19 used for energy generation. In the post-processing network, change in the number abundance Y_i of an isotope i due to convective transport and nuclear burning is modeled by

$$\frac{\mathrm{d}Y_i}{\mathrm{d}t} = \left(\frac{\partial Y_i}{\partial t}\right)_{\rm nuc} + \frac{\partial}{\partial M}\left[(4\pi r^2\rho)^2 D_{\rm MLT}\frac{\partial Y_i}{\partial M}\right], \quad (2)$$

where the first term on the right-hand side is due to nuclear burning and the second due to convective transport, ρ is the density, M is the mass enclosed within radius r, and $D_{\rm MLT}$ is the MLT diffusion coefficient calculated with energy generation from APPROX19. The above treatment is very similar to using the values of $D_{\rm MLT}$ before the proton ingestion for the subsequent proton transport as done in Herwig et al. (2011), where a delayed split of the convective zone was included as an option. We do not attempt to model any delayed split in our calculations. We note that the majority of the ingested protons can travel to the bottom of the He shell within ~ 10 min in our models and any split after this time would not affect the neutron production.

Because proton ingestion is not coupled to energy generation in our calculations, a necessary condition for this approximate treatment is

$$\epsilon_{\rm nuc}\tau_{\rm conv} \ll E_{\rm int}, \quad (3)$$

where $\epsilon_{\rm nuc}$ is the specific rate of energy generation from proton burning, $\tau_{\rm conv}$ is the convective mixing timescale, and $E_{\rm int}$ is the specific internal energy typical of the convective region. Following Jones et al. (2016), we take

$$\tau_{\rm conv} \approx \frac{H_{\rm P}}{v_{\rm conv}}, \quad (4)$$

where the pressure scale height $H_{\rm P}$ and the convective velocity $v_{\rm conv}$ are calculated from the MLT. The post-processing network can accurately calculate the energy generation from the burning of protons as they travel towards the hotter parts of the He shell. We have checked that the condition in Eq. (3) is satisfied for the convective He shell in our models. Take a $25\,{\rm M}_\odot$ model with metallicty $[Z] = -3$ for example. We find that $\tau_{\rm conv} \sim (1\text{–}2)\times 10^4\,{\rm s}$ at central C depletion and $\epsilon_{\rm nuc}\tau_{\rm conv} \lesssim 0.015\,E_{\rm int}$ for all regions in the convective He shell for $M_{\rm p} \lesssim 10^{-4}\,{\rm M}_\odot$. Even for $M_{\rm p} = 10^{-3}\,{\rm M}_\odot$, the highest ingested mass considered in this study, $\epsilon_{\rm nuc}\tau_{\rm conv} \lesssim 0.06\,E_{\rm int}$. The above discussion suggests that ignoring energy generation associated with proton ingestion in our models is a reasonable approximation, especially for $M_{\rm p} \lesssim 10^{-4}\,{\rm M}_\odot$.

The approximate treatment of ingestion and transport of protons described above represents a major simplification. Nevertheless, it allows us to calculate the nucleosynthesis across multi-zones in the convective He shell within the limitations of 1D stellar models. We prefer this treatment to one-zone calculations although we expect qualitatively similar results for similar conditions.

3. RESULTS

The proton ingestion initiates a sequence of reactions producing neutrons, which are captured to make heavy elements. Below we present the results for a $25\,{\rm M}_\odot$ star with varying initial metallicity. For each case, we compute the full evolution and the associated nucleosynthesis of the star from its birth until its death in a CCSN. The explosion subsequent to core collapse is simulated by driving a piston outwards from the base of the O shell. The piston velocity is adjusted so that the desired explosion energy is obtained. The material inside the initial radius of the piston is assumed to fall back immediately onto the protoneutron star produced by the core collapse. The final yields are calculated by assuming that all the material outside this radius is ejected.

3.1. *Neutrons from Proton Ingestion and Neutron-Capture Nucleosynthesis*

At the top of the convective He shell where protons are ingested, the temperature is $T \sim 10^8\,{\rm K}$ and the density is $\rho \sim 50\,{\rm g\,cm^{-3}}$. In comparison, the conditions at the bottom of this shell are $T \sim 2.7\times 10^8\,{\rm K}$ and $\rho \sim 500\,{\rm g\,cm^{-3}}$. The shell also has traces of primary ^{12}C and ^{16}O with mass fractions of $\sim 5\times 10^{-2}$ and $\sim 2\times 10^{-3}$, respectively, produced by He burning. As the ingested protons are transported to the hotter region, they are captured by ^{12}C to produce ^{13}N, which decays to ^{13}C on a time scale of $\sim 863\,{\rm s}$. Neutrons are released from the subsequent reaction $^{13}{\rm C}(\alpha,{\rm n})^{16}{\rm O}$. The occurrence of the above processes can be clearly seen from Fig. 2, which shows the abundance profiles of neutrons, protons, ^{13,14}C, ^{13,14,15}N, and ^{17}O in the He shell at different times after $10^{-4}\,{\rm M}_\odot$ of protons are ingested at central C depletion in a primordial $25\,{\rm M}_\odot$ star. In general, the composition at a specific mass coordinate in the He shell changes as a result of both convective mixing and nuclear reactions [see Eq. (2)]. Sufficiently small time steps are required to follow these changes accurately. We find that limiting the maximum time step

to 100 s is adequate to calculate the nucleosynthesis resulting from proton ingestion.

For illustration (see Fig. 3), we describe the generic evolution of the neutron (number) density $n_{\rm n}$ in a zone (with a fixed mass coordinate) near the bottom of the convective He shell after $10^{-4}\,{\rm M}_\odot$ of protons are ingested at the top. Transport of ingested protons to the zone and the associated production of ^{13}C take $\sim 10^4$ s. Then $n_{\rm n}$ sharply increases because neutron production by $^{13}{\rm C}(\alpha,{\rm n})^{16}{\rm O}$ occurs efficiently at the relatively high temperature of the zone. The primary ^{16}O from He burning is the main neutron poison through $^{16}{\rm O}({\rm n},\gamma)^{17}{\rm O}$. The other significant neutron poison is ^{14}N produced by $^{13}{\rm C}({\rm p},\gamma)^{14}{\rm N}$ following proton ingestion. The competition between neutron production and capture results in a high plateau of $n_{\rm n} \sim (3$–$5) \times 10^{14}\,{\rm cm}^{-3}$. This high plateau is maintained for $\sim 10^5$ s until ^{13}C is burned away. Subsequently $n_{\rm n}$ decreases until a low plateau at $n_{\rm n} \sim 10^{11}\,{\rm cm}^{-3}$ is reached on a time scale of $\sim 10^6$ s. This low plateau is established through competition between neutron production by $^{17}{\rm O}(\alpha,{\rm n})^{20}{\rm Ne}$ and capture by the primary ^{12}C and ^{16}O, and is maintained for $\sim 10^7$ s. The final evolution of $n_{\rm n}$ mainly follows the rate of $^{17}{\rm O}(\alpha,{\rm n})^{20}{\rm Ne}$, which in turn follows the temperature of the zone with some significant drop near the end of the star's life due to expansion after core C depletion and an eventual sharp rise due to contraction in the last $\sim (2$–$3) \times 10^5$ s before core collapse. We note that ^{22}Ne is also produced by $^{14}{\rm N}(\alpha,\gamma)^{18}{\rm F}(e^+\nu_e)^{18}{\rm O}(\alpha,\gamma)^{22}{\rm Ne}$ in the He shell due to proton ingestion. Neutron production by $^{22}{\rm Ne}(\alpha,{\rm n})^{25}{\rm Mg}$, however, is negligible compared to that by $^{13}{\rm C}(\alpha,{\rm n})^{16}{\rm O}$ and $^{17}{\rm O}(\alpha,{\rm n})^{20}{\rm Ne}$.

Figure 4a compares the detailed evolution of $n_{\rm n}$ in the above zone when different amounts of protons are ingested in a $25\,{\rm M}_\odot$ star with zero metallicity. For an ingested proton mass of $M_{\rm p} \lesssim 5 \times 10^{-5}\,{\rm M}_\odot$, the high plateau of $n_{\rm n}$ decreases monotonically with $M_{\rm p}$. For $M_{\rm p} \lesssim 10^{-6}\,{\rm M}_\odot$, however, the peak $n_{\rm n}$ is so low that nucleosynthesis by neutron capture effectively ceases. On the other hand, for $M_{\rm p} > 10^{-4}\,{\rm M}_\odot$, abundant protons start to produce significant amounts of ^{14}N through $^{13}{\rm C}({\rm p},\gamma)^{14}{\rm N}$, which then drives down $n_{\rm n}$ through $^{14}{\rm N}({\rm n},{\rm p})^{14}{\rm C}$. The effect of increased ^{14}N is somewhat offset by higher ^{13}C production such that neutron capture is still efficient for $M_{\rm p} \sim 10^{-3}$. Overall, we find that for $10^{-5}\,{\rm M}_\odot \lesssim M_{\rm p} \lesssim 10^{-3}\,{\rm M}_\odot$, neutron capture is efficient with total neutron exposures of $\int n_{\rm n} v_{\rm n}\,{\rm d}t \sim 15$–$45\,({\rm mb})^{-1}$, where $v_{\rm n}$ is the thermal velocity of neutrons. This neutron capture results in production of heavy elements up to Bi with ${\rm [Sr/Ba]} \lesssim -0.5$ and with a comparable and sometimes higher amount of Pb relative to Ba. For $10^{-6}\,{\rm M}_\odot \lesssim M_{\rm p} < 10^{-5}\,{\rm M}_\odot$, neutron capture is much less efficient but can still produce a reasonable amount of Sr with low Ba (${\rm [Sr/Ba]} > -0.5$) and negligible Pb (see Fig. 5 and Table 2).

The metallicity of the star has little effect on the neutron density $n_{\rm n}$ for $[Z] \lesssim -2$ for a fixed $M_{\rm p}$ (see Fig. 4b). This is because the main neutron poison is the primary ^{16}O from He burning in He shells of such low metallicities. As $[Z]$ increases beyond -2, however, the peak $n_{\rm n}$ and the duration of the high plateau start to decrease due to the increasing amount of poisons in the star's birth material. This results in decreasing efficiency of nucleosynthesis by neutron capture with increasing metallicity. Nevertheless, such nucleosynthesis is still efficient up to $[Z] \sim -1$, producing mainly Sr along with elements up to around Ba. The corresponding yields for $M_{\rm p} \gtrsim 5 \times 10^{-5}\,{\rm M}_\odot$ can be higher than those for the well-known weak s-process (Käppeler et al. 2011) at such metallicities (see §3.6 and Table 2).

We note that the values of $n_{\rm n}$ achieved during the high plateau correspond to typical i-process neutron densities, which have also been found in one-zone calculations of nucleosynthesis from proton ingestion in low to intermediate-mass stars (Dardelet et al. 2014) and in multi-zone calculations for similar environments (Herwig et al. 2011; Denissenkov et al. 2017). Whereas such n_n values are determined ultimately by the relevant nuclear physics and astrophysical conditions, it is important to understand how similar conditions can be achieved in different environments, which may have very distinct implications for chemical evolution. On the other hand, the values of $n_{\rm n}$ achieved during the low plateau is consistent with s-process neutron densities. Incidentally, $^{17}{\rm O}(\alpha,{\rm n})^{20}{\rm Ne}$, which is responsible for maintaining the neutron density during this phase, is also known to be important for the weak s-process in massive stars at low metallicites (Baraffe et al. 1992) and in spinstars (Pignatari et al. 2008; Frischknecht et al. 2016). Whereas neutrons are generated by $^{22}{\rm Ne}(\alpha,{\rm n})^{25}{\rm Mg}$ in the latter two cases, $^{17}{\rm O}(\alpha,{\rm n})^{20}{\rm Ne}$ serves to recover the neutron captured by ^{16}O, thereby effectively reducing its neutron-capture capability by a factor of $\kappa \sim 13$–15. This effect is achieved because the rate of $^{17}{\rm O}(\alpha,{\rm n})^{20}{\rm Ne}$ is higher than that of $^{17}{\rm O}(\alpha,\gamma)^{21}{\rm Ne}$ by a factor of κ at temperatures of $\sim (2.5$–$3) \times 10^8$ K typical of the weak s-process.

3.2. *Neutron Capture in Metal-Poor Massive Stars*

Based on the preceding discussion, metal-poor stars with $[Z] \lesssim -2$ but non-zero metallicities have similarly high plateaus of $n_{\rm n}$. Starting from the Fe group nuclei in their birth material, nucleosynthesis by neutron

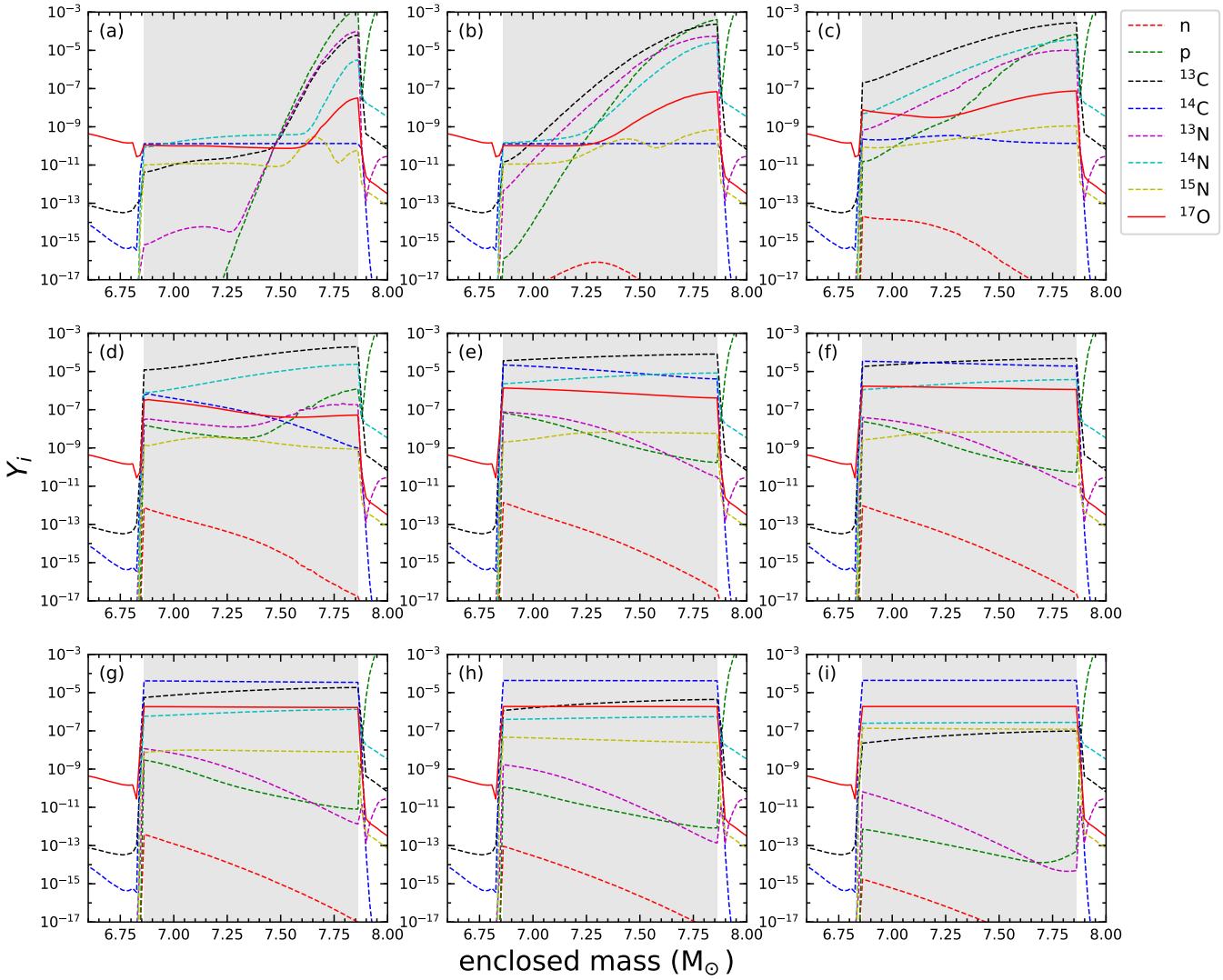

Figure 2. Abundances of neutrons (*dashed red*), protons (*dashed green*), ^{13}C (*dashed black*), ^{14}C (*dashed blue*), ^{13}N (*dashed magenta*), ^{14}N (*dashed cyan*), ^{15}N (*dashed yellow*), and ^{17}O (*solid red*) as functions of mass coordinate at different times t after $10^{-4}\,M_\odot$ of protons are ingested at central C depletion in a metal-free $25\,M_\odot$ star: (a) $t = 8.95 \times 10^2$ s, (b) $t = 3.90 \times 10^3$ s, (c) $t = 9.90 \times 10^4$ s, (d) $t = 2.39 \times 10^4$ s, (e) $t = 1.04 \times 10^5$ s, (f) $t = 2.04 \times 10^5$ s, (g) $t = 3.54 \times 10^5$ s, (h) $t = 5.54 \times 10^5$ s, and (i) $t = 1.06 \times 10^6$ s. The convective He shell is indicated by the grey region.

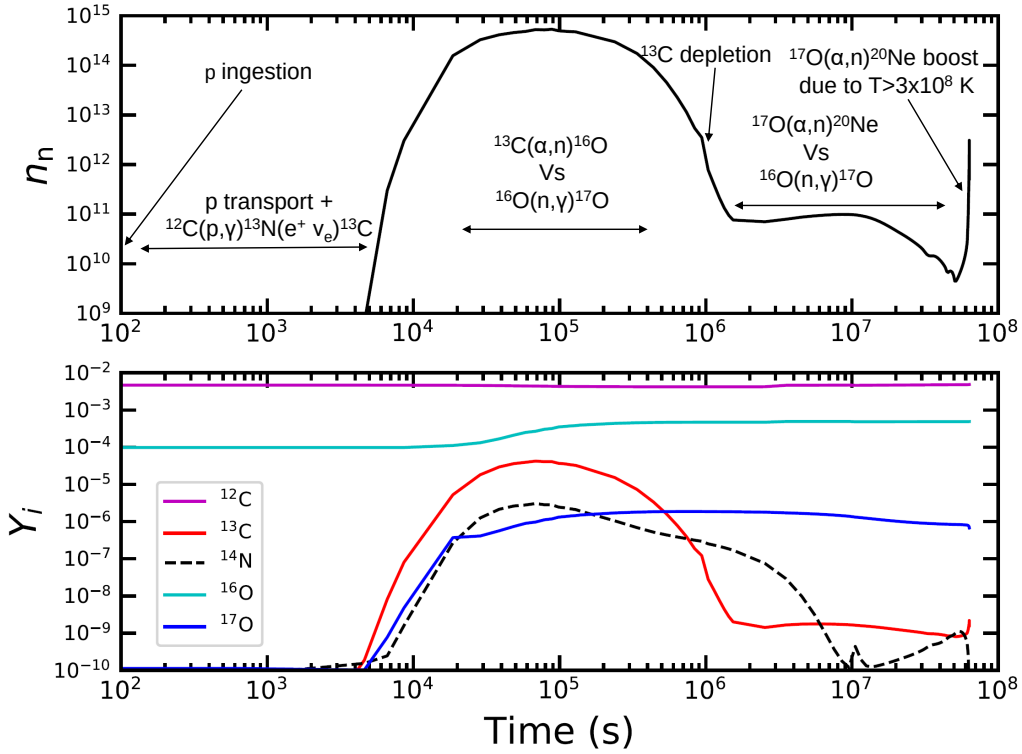

Figure 3. (Top) Neutron density $n_{\rm n}$ in a single zone at the base of the He shell of a metal-free $25\,{\rm M}_\odot$ star as a function of time after $10^{-4}\,{\rm M}_\odot$ of protons are ingested at central C depletion. Various processes determining $n_{\rm n}$ are indicated. (Bottom) Corresponding evolution of the abundance Y_i for ^{12}C (*magenta*), ^{13}C (*red*), ^{14}N (*black*), ^{16}O (*cyan*), and ^{17}O (*blue*).

capture readily produces heavy elements beyond Fe up to Bi. As the initial metallicity increases from zero to $[Z] \sim -2$, more seeds become available, and therefore, the amount of neutron-capture elements produced also increases. For convenience of comparison with observational data, we use [Ba/Eu] as a proxy for the abundance pattern produced. For reference, contributions to the solar abundances from the main *s*-process in AGB stars are characterized by $[{\rm Ba/Eu}]_{\rm s} \sim 1.6$, whereas those from the *r*-process by $[{\rm Ba/Eu}]_{\rm r} \sim -0.8$.

Most of the nucleosynthesis is associated with the high plateau of $n_{\rm n}$ and occurs during the first $\sim 10^6$ s after the proton ingestion. This stage contributes $\sim 98\,\%$ of the total neutron exposure. For $10^{-5}\,{\rm M}_\odot \lesssim M_{\rm p} \lesssim 10^{-3}\,{\rm M}_\odot$, the production pattern during this stage with $n_{\rm n} \sim (3$–$5) \times 10^{14}\,{\rm cm}^{-3}$ has the lowest [Ba/Eu], as low as ~ 0.3, which lies between $[{\rm Ba/Eu}]_{\rm r}$ and $[{\rm Ba/Eu}]_{\rm s}$. When $n_{\rm n}$ drops to $\sim 10^{11}\,{\rm cm}^{-3}$ corresponding to the low plateau, however, neutron capture can still continue for $\gtrsim 10^7$ s. During this time, abundance peaks at Sr, Ba, and Pb corresponding to nuclei with magic neutron numbers $N = 50$, 82, and 126 grow marginally due to very low neutron exposure, whereas the pattern between the peaks evolves considerably to resemble that of a main *s*-process. For example, [Ba/Eu] can increase to ~ 1.1. The sharp rise in $n_{\rm n}$ during the last $\sim$ (2–3) $\times\, 10^5$ s does not contribute much to the total yield or the abundance peaks, but changes the abundances of those elements close to the peaks, such as La and Eu. As a result, [Ba/Eu] can change to ~ 0.9 due to increase in the Eu abundance. Figure 6 shows the abundance patterns produced by neutron capture at different times after $10^{-4}\,{\rm M}_\odot$ of protons are ingested at central C depletion in a $25\,{\rm M}_\odot$ star with $[Z] = -3$.

The above discussion assumes that protons are ingested when C is depleted in the center of the star. In order to explore nucleosynthesis from proton ingestion at a later time, we ingest protons when O is depleted in the center and repeat the calculations. For our $25\,{\rm M}_\odot$ models, the time of ingestion is $\sim 10^6$ s prior to core collapse. The evolution of $n_{\rm n}$ is similar to the case of proton ingestion at central C depletion, with a high plateau at $n_{\rm n} \sim (3$–$5) \times 10^{14}\,{\rm cm}^{-3}$ lasting $\sim 10^5$ s and a sharp rise near the end of the star's life, except that there is not a low plateau but only a dip at $n_{\rm n} \sim 10^{11}{\rm cm}^{-3}$ prior to the sharp rise (see Fig. 7). Based on the discussion above, the corresponding nucleosynthesis should produce similar relative abundance peaks but significantly different patterns between the peaks compared to the case of proton ingestion at central C depletion. Specifically, the

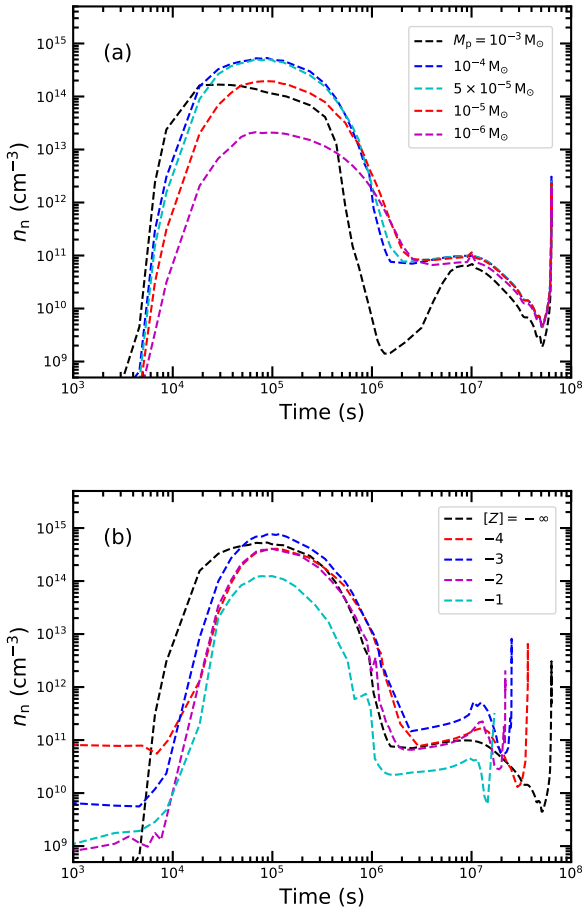

Figure 4. Neutron density n_n in a single zone at the base of the He shell of a $25\,M_\odot$ star with metallicity $[Z]$ as a function of time after a total mass M_p of protons are ingested at central C depletion. (a) Cases of $M_p = 10^{-3}$ (*black*), 10^{-4} (*blue*), 5×10^{-5} (*cyan*), 10^{-5} (*red*), and $10^{-6}\,M_\odot$ (*magenta*), all for zero metallicity. (b) Cases of zero metallicity (*black*), $[Z] = -4$ (*red*), -3 (*blue*), -2 (*magenta*), and -1 (*cyan*), all for $M_p = 10^{-4}\,M_\odot$.

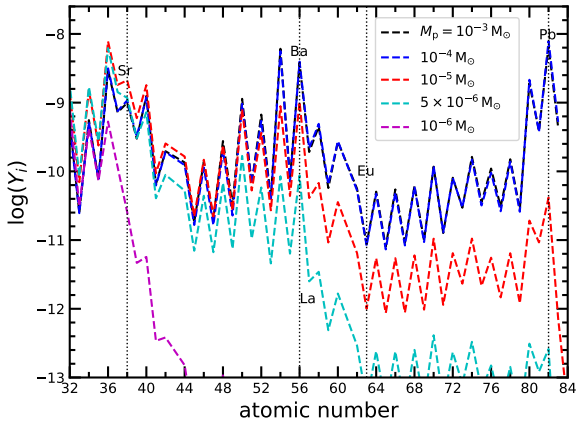

Figure 5. Yield patterns for a $25\,M_\odot$ star with $[Z] = -3$ and ingestion of $10^{-3}\,M_\odot$ (*black*), $10^{-4}\,M_\odot$ (*blue*), $10^{-5}\,M_\odot$ (*red*), $5\times10^{-6}\,M_\odot$ (*cyan*), and $10^{-6}\,M_\odot$ (*magenta*) of protons at central C depletion. Note that the black and blue curves are indistinguishable.

lack of an extended low n_n plateau in the present case results in a lower [Ba/Eu] of ~ 0.6 (see Fig. 8). As a limit for cases of later proton ingestion, [Ba/Eu] could be as low as ~ 0.3 if nucleosynthesis occurs entirely during the phase of the high n_n plateau.

Therefore, the detailed abundance pattern produced by neutron capture in metal-poor massive stars is sensitive to the total duration Δ from the time of proton ingestion until core collapse. In general, $\Delta \lesssim 10^6$ s produces [Ba/Eu] $\lesssim 0.6$ because the low neutron density phase is avoided. On the other hand, for $\Delta > 10^6$ s, [Ba/Eu] progressively increases towards the *s*-process value. This suggests that proton ingestion leading to $n_n \gtrsim 10^{14}\,\mathrm{cm}^{-3}$ typical of the *i*-process may not necessarily produce [Ba/Eu] values corresponding to the *r*/*s* stars. The initial phase of high neutron density is usually followed by a low neutron density phase, which can be avoided only if nucleosynthesis is terminated after the initial phase. In massive stars, this termination can happen naturally due to the onset of core collapse. In other scenarios of the *i*-process such as associated with low and intermediate-mass stars, the mechanism for the termination would be very different. Regardless of the mechanism, the timescale for shutting down nucleosynthesis has to be $\ll 10^7$ s in order to retain [Ba/Eu] $\lesssim 0.6$.

We calculate the nucleosynthesis for four models of a $25\,M_\odot$ star (see Table 3) and compare the results with data on four VMP stars in Fig. 9. These models differ in metallicity $[Z]$, ingested proton mass M_p, ingestion time t_{ing}, and CCSN explosion energy E_{expl}. Models 1, 2, 3, and 4 have ($[Z]$, $M_p/M_\odot$, t_{ing}, E_{expl}/ergs) = (-3, 5×10^{-5}, Cdep, 10^{50}), (-3, 10^{-4}, Cdep, 10^{50}), (-3, 10^{-4}, Odep, 10^{50}), and (-4, 10^{-4}, Odep, 3×10^{50}), respectively, where Cdep and Odep stand for central C ($\Delta \sim 3\times10^7$ s) and O ($\Delta \sim 10^6$ s) depletion, respectively. The $[Z]$ is chosen to be consistent with the [Fe/H] of the comparison star, and the E_{expl} to provide the plausible dilution mass for accommodating the observed absolute abundances (see §4). For the chosen E_{expl}, the CCSN explosion has little effect on the yields of neutron-capture elements but can cause a minor decrease in [Ba/Eu] by ~ 0.1 (see §3.5 and Tables 2–3). Figure 9 shows that the patterns from Ba to Pb produced by the models are in excellent agreement with

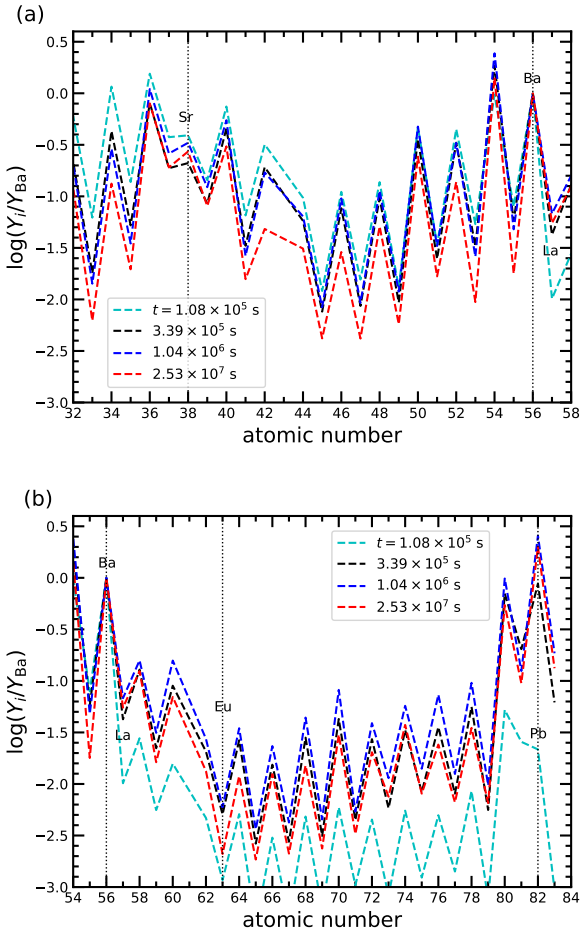

Figure 6. (a) Yield pattern from Ge to Ce normalized to Ba for a $25\,M_\odot$ star with $[Z] = -3$ at time $t = 1.08 \times 10^5$ s (*cyan*), 3.39×10^5 s (*black*), 1.04×10^6 s (*blue*), and 2.53×10^7 s (*red*, just before core collapse) after $10^{-4}\,M_\odot$ of protons are ingested at central C depletion. (b) Same as (a) but showing yield pattern from Xe to Bi.

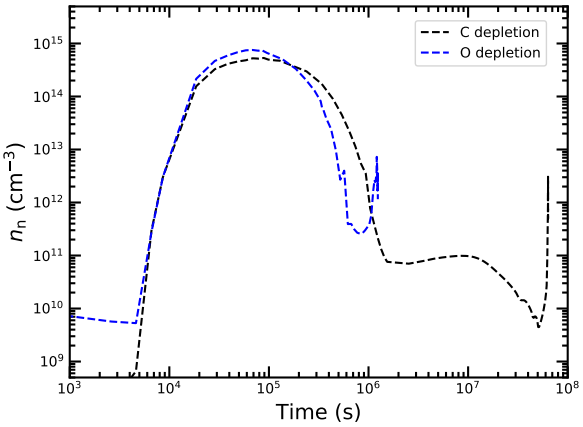

Figure 7. Neutron density n_n in a single zone at the base of the He shell of a metal-free $25\,M_\odot$ star as a function of time after $10^{-4}\,M_\odot$ of protons are ingested at central O depletion (*blue*) compared to that for ingestion at central C depletion (*black*).

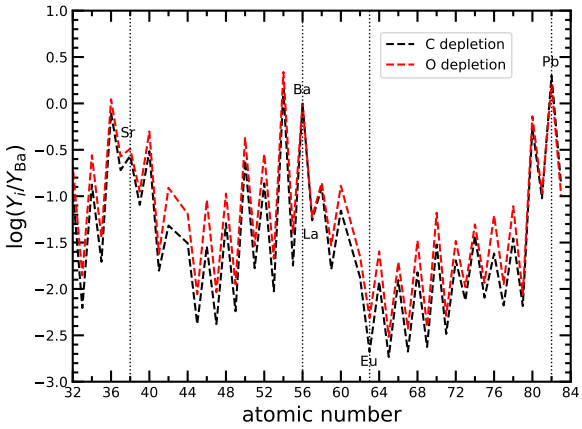

Figure 8. Yield pattern normalized to Ba for a $25\,M_\odot$ star with $[Z] = -3$ and ingestion of $10^{-4}\,M_\odot$ of protons at central C depletion (*black*) compared to that for ingestion at central O depletion (*red*).

the data on the four VMP stars. Similar agreement is also found for other VMP stars (see Fig. 10).

As mentioned above, because n_n is nearly independent of metallicity for $[Z] \lesssim -2$, the total yield of heavy elements is proportional to the amount of seeds inherited from the initial metallicity (see Fig. 11a). This relation between the yield and metallicity, however, breaks down for primordial massive stars with zero metallicity, which we discuss below.

3.3. *Neutron Capture in Metal-Free Massive Stars*

Because the birth material of primordial stars is free of metals that can serve as seeds for neutron capture, no significant heavy element synthesis is expected even though n_n values are almost identical to those in their metal-poor counterpart with $[Z] \lesssim -2$. Interestingly, however, tiny amounts of Ca isotopes (with a mass fraction of $\sim 10^{-10}$ for ^{40}Ca and $\sim 10^{-11}$ for ^{44}Ca) and even less amounts of Ti isotopes (with mass fractions of $\sim 10^{-12}$ for ^{46}Ti to ^{50}Ti) produced by the hot CNO cycle (Keller et al. 2014) are present in the He shell, and these primary nuclei act as the seeds. Because most of the seeds (^{40}Ca) have the magic neutron number $N = 20$, production of heavy elements beyond Fe is greatly slowed down due to the bottleneck at the next magic number $N = 28$. We find that even with the n_n of the high plateau, clearing this bottleneck takes most of the duration ($\sim 10^5$ s) of this plateau, which limits the

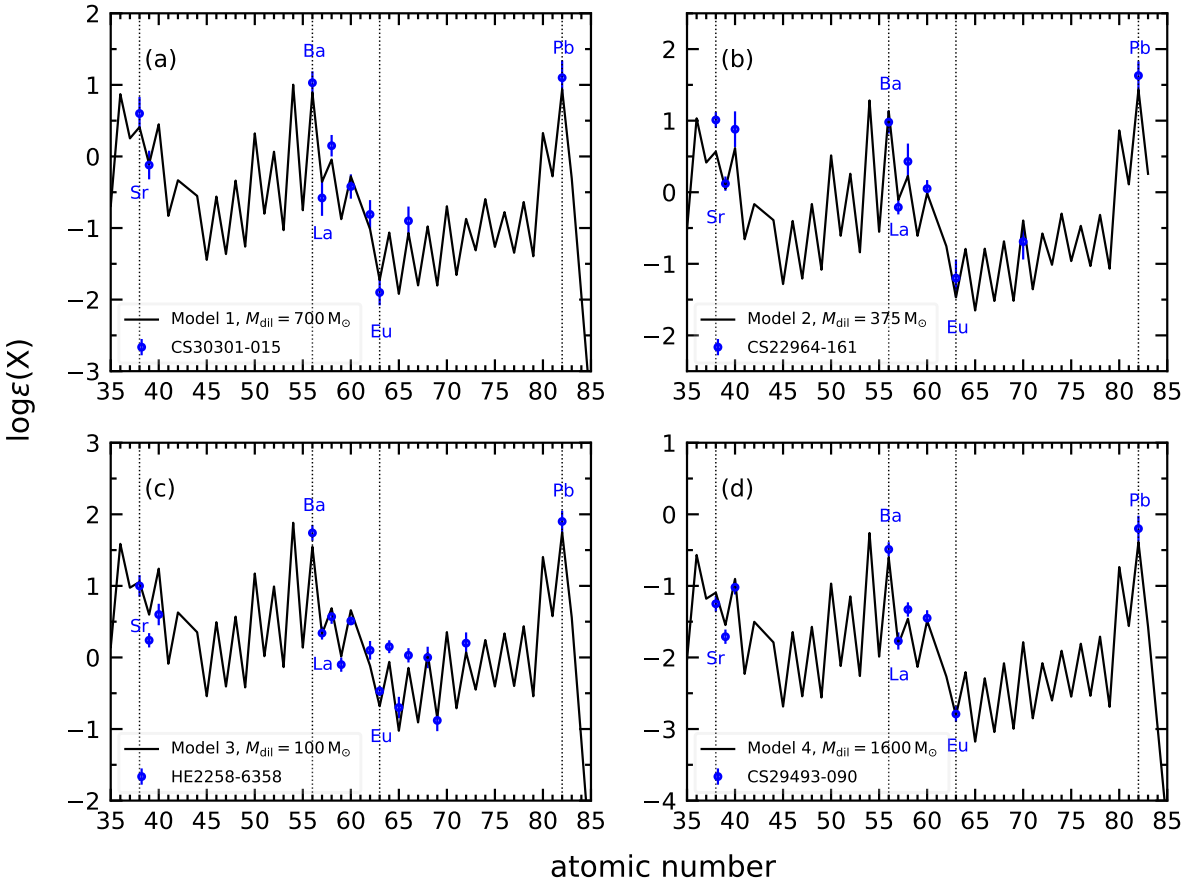

Figure 9. Comparison of model yields with abundances in VMP stars. All models are for a $25\,M_\odot$ star but differ in metallicity $[Z]$, ingested proton mass M_p, ingestion time t_{ing}, and explosion energy E_{expl}. Models 1, 2, 3, and 4 have ($[Z]$, $M_p/M_\odot$, t_{ing}, E_{expl}/ergs) = (-3, 5×10^{-5}, Cdep, 10^{50}), (-3, 10^{-4}, Cdep, 10^{50}), (-3, 10^{-4}, Odep, 10^{50}), and (-4, 10^{-4}, Odep, 3×10^{50}), respectively, where Cdep (Odep) stands for central C (O) depletion. Data are given as $\log\epsilon(X) \equiv \log(X/H) + 12$ for element X. (a) Model 1 and CS 30301-015 (Aoki et al. 2002) for a dilution mass of $M_{dil} = 700\,M_\odot$. (b) Model 2 and CS 22964-161 (Thompson et al. 2008) for $M_{dil} = 375\,M_\odot$. (c) Model 3 and HE 2258-6358 (Placco et al. 2013) for $M_{dil} = 100\,M_\odot$. (d) Model 4 and CS 29493-090 (Spite et al. 2014) for $M_{dil} = 1{,}600\,M_\odot$.

production of heavy elements. Nevertheless, elements up to Bi can be produced, with their yields particularly sensitive to the peak n_n, and hence the ingested proton mass M_p (see Fig. 4a). The maximum yields occur for $M_p \sim 10^{-4}\,M_\odot$ but are ~ 500 times lower than the yields of the $[Z] = -5$ counterpart or comparable to those of the $[Z] \sim -7.5$ counterpart for the same M_p. Nonetheless, metal-free stars with $M_p \sim 10^{-4}\,M_\odot$ can provide the lowest amounts of neutron-capture elements measured in VMP stars (see §4).

In sharp contrast to metal-poor massive stars, metal-free ones leave most of the seeds unused even for $M_p \sim 10^{-4}\,M_\odot$ with the highest efficiency of neutron capture. In addition, fresh seeds are produced by neutron capture on the primary ^{22}Ne, which has a mass fraction of $\sim 2\times10^{-7}$ in the He shell. Were more episodes of proton ingestion to occur in metal-free massive stars, the unused and freshly-synthesized seeds could be utilized to increase the yields of heavy elements dramatically (see §3.4). For example, three episodes with $M_p = 10^{-4}\,M_\odot$ for each would increase the yields by ~ 10 times.

As mentioned above, Clarkson et al. (2018) found that an *i*-process could result from proton ingestion in the convective He shell in a zero-metallicity star of $45\,M_\odot$. In their study based on the MESA code, a substantial amount of proton ingestion occurs just after the end of core He burning when the convective He shell exchanges material with the H-rich layers. This large

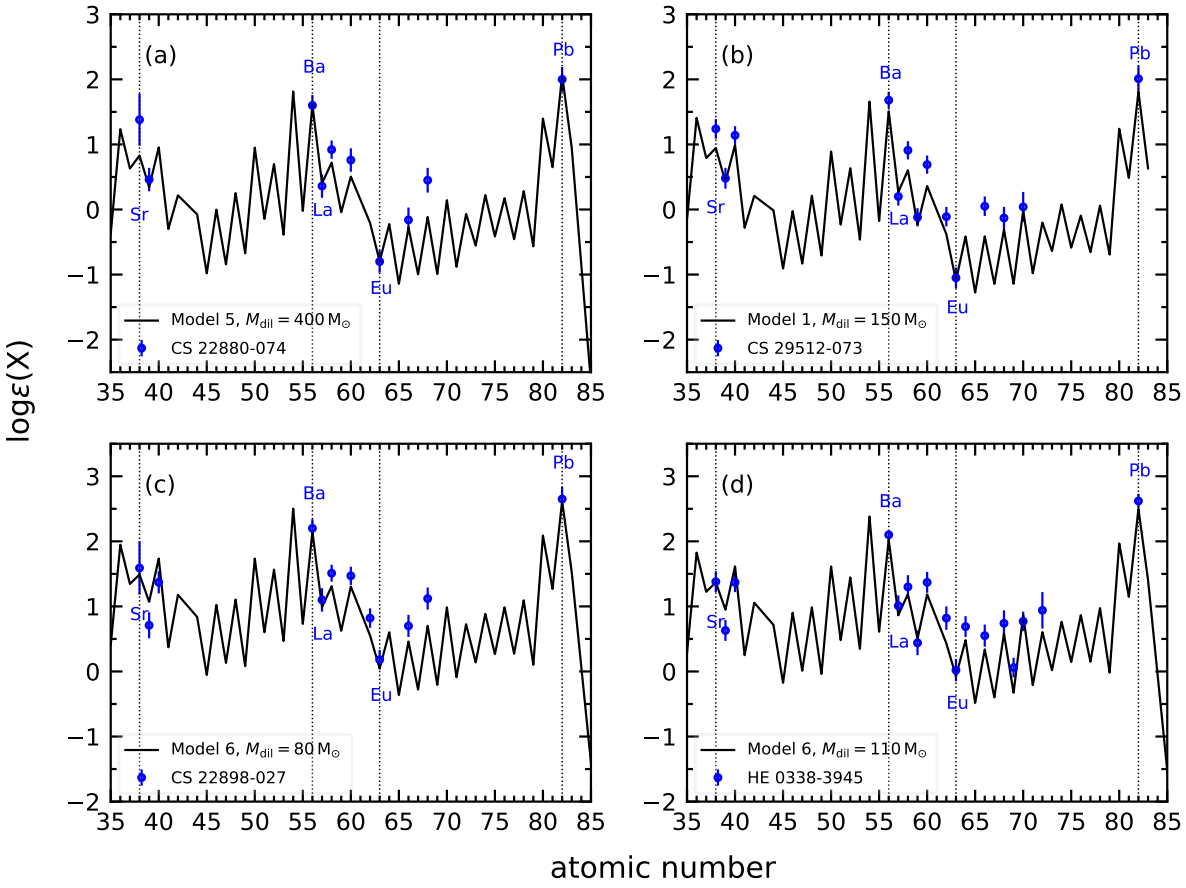

Figure 10. More comparison of model yields with abundances in VMP stars. See Table 3 for description of models. (a) Model 5 and CS 22880-074 (Aoki et al. 2002) for a dilution mass of $M_{\rm dil} = 400\,{\rm M}_\odot$. (b) Model 1 and CS 29512-073 (Roederer et al. 2014b) for $M_{\rm dil} = 150\,{\rm M}_\odot$. (c) Model 6 and CS 22898-027 (Aoki et al. 2002) for $M_{\rm dil} = 80\,{\rm M}_\odot$. (d) Model 6 and HE 0338-3945 (Jonsell et al. 2006) for $M_{\rm dil} = 110\,{\rm M}_\odot$.

proton ingestion leads to large energy generation with $\epsilon_{\rm nuc}\tau_{\rm conv} \approx 0.26\,E_{\rm int}$. In their one-zone nucleosynthesis calculations, the initial proton mass fraction was taken to be 1 %, which produced a peak $n_{\rm n}$ of $\approx 6\times10^{13}\,{\rm cm}^{-3}$. This value is approximately an order of magnitude lower than the highest $n_{\rm n}$ found in the present study. The difference is simply due to the larger proton ingestion used in Clarkson et al. (2018). For example, $M_{\rm p} \lesssim 10^{-4}\,{\rm M}_\odot$ in our calculations corresponds to a proton mass fraction of $\lesssim 0.01$ % for a single-zone calculation, to be compared with 1 % adopted by Clarkson et al. (2018). A mass fraction of 1 % would correspond to $M_{\rm p} \sim 10^{-2}\,{\rm M}_\odot$ for our study. As discussed above, for $M_{\rm p} \gtrsim 10^{-3}\,{\rm M}_\odot$, substantial amounts of ^{14}N are produced to make ^{14}N the dominant neutron poison, which lowers the neutron abundance through $^{14}{\rm N(n,p)}^{14}{\rm C}$.

3.4. *Multiple Episodes of Proton Ingestion*

With the overshoot prescription described in §2, we found that subsequent to the proton ingestion at central C depletion, additional ingestion occurred at central O and Si depletion, especially for stars with $[Z] \lesssim -4$. Because each episode of proton ingestion with $10^{-5}\,{\rm M}_\odot \lesssim M_{\rm p} \lesssim 10^{-3}\,{\rm M}_\odot$ leads to a period of high neutron density, multiple episodes of ingestion can significantly increase the efficiency of neutron-capture nucleosynthesis. This is particularly relevant for metal-free stars, where a substantial amount of the seeds are left behind and additional seeds are produced by neutron capture following a single episode of proton ingestion. For these stars, with each additional episode of proton ingestion, the yields of heavy elements increase substantially as the unused seeds from the previous episode are utilized.

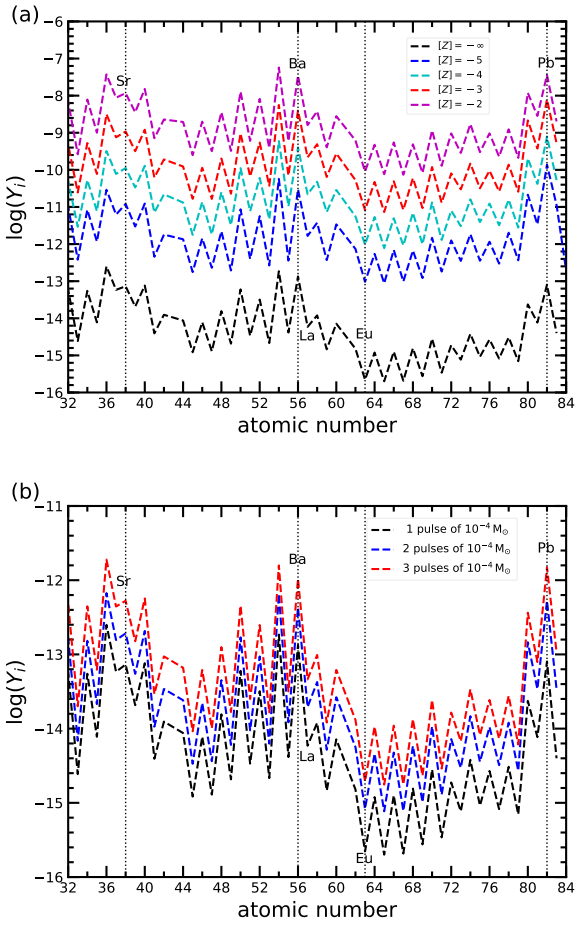

Figure 11. (a) Yield patterns for a $25\,M_\odot$ star with ingestion of $10^{-4}\,M_\odot$ of protons at central C depletion for zero metallicity (*black*), $[Z] = -5$ (*blue*), -4 (*cyan*), -3 (*red*), and -2 (*magenta*). (b) Yield pattern for the zero-metallicity case (*black*) in (a) compared to those for 2 (blue) and 3 (red) pulses of ingestion with $M_p = 10^{-4}\,M_\odot$ for each pulse and an interval of 10^6 s between successive pulses starting at central C depletion.

We explored multiple episodes of proton ingestion for a metal-free star by injecting two or three pulses of protons with $M_p = 10^{-4}\,M_\odot$ for each pulse and an interval of 10^6 s between successive pulses starting at central C depletion. The yields of heavy elements increased by a factor of ~ 4 or 10, respectively, compared to the case of a single pulse (see Table 2 and Fig. 11b). For metal-poor stars, most of the seeds were used up after a single pulse with $M_p \gtrsim 10^{-5}\,M_\odot$. Additional pulses could increase the yield of Pb relative to Ba and Sr (see Models 5 and 6 in Table 3), thereby providing overall patterns in excellent agreement with data on some CEMP-*s* and CEMP-*r*/*s* stars that are enhanced in Pb (see Fig. 10).

3.5. *Effect of the CCSN Shock*

As the shock goes through the He shell, it raises the temperature of the material there so that a short burst of neutrons may be released via (α, n) reactions on ^{13}C, ^{17}O, and ^{22}Ne, which have been produced earlier due to proton ingestion. The subsequent neutron capture can affect the final [Ba/Eu]. The amount of neutrons released depends on the explosion energy, which controls the peak temperature of the shocked material and hence the rate of the relevant (α, n) reactions. For an explosion energy of $E_{expl} = 1.2 \times 10^{51}$ ergs, we found that the yield of Eu increased by a factor of ~ 2 but that of Ba was virtually unchanged, resulting in a decrease of [Ba/Eu] by ~ 0.3 compared to the pre-shock value. For lower E_{expl} of 10^{50} and 3×10^{50} ergs, release of neutrons by the shock was so inefficient that [Ba/Eu] only increased by ~ 0.05 and 0.1, respectively, after passage of the shock.

3.6. *Neutron Capture in a* $25\,M_\odot$ *Star with* $[Z] = -1$

In addition to models with initial metallicity up to $[Z] = -2$, we also calculated the nucleosynthesis in a $25\,M_\odot$ star with $[Z] = -1$. In this case, the initial metal composition was scaled from the solar abundances for all the corresponding elements up to Bi. The effect of neutron poisons inherited from the initial metallicity is evident from the lower neutron density compared to the $[Z] \lesssim -2$ models (see Fig. 4b). The final yields of heavy elements in this case include the contributions from the initial metallicity and the weak *s*-process in addition to what is produced due to proton ingestion (see Table 2). We found that neutron capture was most efficient for an ingested proton mass of $M_p \sim 10^{-3}\,M_\odot$, producing substantial amounts of Sr and Ba. Efficiency of neutron capture decreased rapidly for lower amounts of proton ingestion, with production of mostly Sr. Nevertheless, for $M_p \gtrsim 5 \times 10^{-5}\,M_\odot$, the production of Sr due to proton ingestion still exceeds that by the weak *s*-process (see Table 2). Therefore, nucleosynthesis from proton ingestion in massive stars is expected to have an important effect on Galactic chemical evolution of heavy elements at least up to [Fe/H] ~ -1.

4. IMPLICATIONS FOR OBSERVATIONS OF VMP STARS

Based on exploration with 1D models, we have proposed a new site for neutron-capture nucleosynthesis in early stars of ~ 20–$30\,M_\odot$. This nucleosynthesis results from proton ingestion in convective He shells and has characteristics ranging from those of the *i*-process, which has been studied in connection with proton ingestion in stars of $< 10\,M_\odot$, to those of the main *s*-process in low and intermediate-mass stars as well as those of the

weak s-process in massive stars. Our calculations suggest that the proposed neutron-capture site can resolve a number of observational puzzles pertaining to VMP stars. Before we discuss these implications in detail, we summarize the features of this site that are important in comparison with observations.

The amount of heavy elements produced from proton ingestion in an early massive star depends mainly on the ingested proton mass $M_{\rm p}$ and the amount of seeds inherited from its initial metallicity $[Z] \sim$ [Fe/H]. For [Fe/H] $\lesssim -2$, the yield scales linearly with the number ratio (Fe/H) except for metal-free stars, where the seeds are the primary Ca and Ti isotopes produced during their evolution. For stars with a specific (including zero) metallicity, neutron capture is efficient for $10^{-5}\,{\rm M}_\odot \lesssim M_{\rm p} \lesssim 10^{-3}\,{\rm M}_\odot$ and is generally characterized by high Ba and Pb production with [Sr/Ba] $\lesssim -0.5$. In contrast, for $10^{-6}\,{\rm M}_\odot \lesssim M_{\rm p} < 10^{-5}\,{\rm M}_\odot$, neutron capture is less efficient with low Ba and Pb production and [Sr/Ba] > -0.5. The yield patterns for $10^{-5}\,{\rm M}_\odot \lesssim M_{\rm p} \lesssim 10^{-3}\,{\rm M}_\odot$ can vary from s-like ([Ba/Eu] > 0.6 for $\Delta > 10^6$ s) to r/s-like ([Ba/Eu] $\lesssim 0.6$ for $\Delta \lesssim 10^6$ s) depending on the time Δ available for neutron capture, with an overall range of [Ba/Eu] $\sim$ 0.2–1.

4.1. *Ubiquity of* Sr *and* Ba

The ubiquity of Sr in VMP stars may not be surprising. Neutrino-driven winds from a protoneutron star created in a CCSN can produce heavy elements up to $A \sim 120$ with $\sim 10^{-8}$–$10^{-7}\,{\rm M}_\odot$ of Sr (Arcones & Montes 2011). When mixed with $\sim 10^2$–$10^4\,{\rm M}_\odot$ of ISM as expected for a wide range of CCSN explosion energy, such yields can explain $\log\epsilon({\rm Sr}) \equiv \log({\rm Sr/H}) + 12 \lesssim 0$ observed in extremely metal-poor stars with [Fe/H] $\lesssim -3.5$ (Suda et al. 2008). Ba is also frequently observed in such stars including several CEMP-no stars. The latter belong to a group with some members considered to have formed from an ISM polluted exclusively by primordial (metal-free) massive stars (Hansen et al. 2016a). This presents a major puzzle because Ba is not produced in neutrino-driven winds and nor is its widespread presence accountable by the r-process in such rare events as neutron star mergers or jet-driven CCSNe. Our proposed site, however, operates in a significant fraction of massive stars even at zero metallicity, so it can provide Ba to stars of the lowest metallicities including CEMP-no stars. Stars with [Fe/H] $\lesssim -3.5$ are observed to have $\log\epsilon({\rm Ba}) \lesssim -1$ with the lowest measured value of ~ -3.9. Our metal-free $25\,{\rm M}_\odot$ models with $M_{\rm p} \sim 10^{-4}\,{\rm M}_\odot$ can provide $\log\epsilon({\rm Ba}) \sim -5$ to -3 if their Ba yields (see Table 2) are diluted by $\sim 10^2$–$10^4\,{\rm M}_\odot$ of ISM. With few additional episodes of proton ingestion, such models can provide $\log\epsilon({\rm Ba})$ up to ~ -2, the maximum Ba enrichment observed in stars with [Fe/H] $\lesssim -4$. Extremely metal-poor massive stars with $-7 \lesssim$ [Fe/H] $\lesssim -4$ can account for $-3 < \log\epsilon({\rm Ba}) \lesssim 0$, which includes the highest Ba enrichment observed in stars with [Fe/H] $\lesssim -3.5$. Therefore, the proposed site in metal-free and metal-poor massive stars can explain adequately the ubiquity of Ba in VMP stars.

4.2. *Diversity of VMP Stars*

We note that the amount of Sr synthesized by neutrino-driven winds is more than that of Sr or Ba by the proposed site for massive stars with [Fe/H] $\lesssim -5$ and comparable to that for [Fe/H] ~ -4 (see Table 2). The Sr from these winds along with the Ba from the proposed site at such metallicities would naturally explain VMP stars with [Sr/Ba] $\gtrsim -0.5$ (Spite et al. 2014; Suda et al. 2008). Were the wind material not ejected such as in a CCSN with weak explosion and hence severe fallback, both the Sr and Ba in the ejecta would be exclusively from the proposed site operating in the He shell, which is expected to be ejected even for weak explosion. In this case, both [Sr/Ba] > -0.5 and [Sr/Ba] $\lesssim -0.5$ can be produced depending on the ingested proton mass, with the latter values consistent with other observations.

With the heavy-element yields proportional to the metallicity for the proposed site, CCSNe from massive stars with $-4 \lesssim$ [Fe/H] $\lesssim -2$ would result in substantially higher enrichment. The level of enrichment also depends on the amount of dilution and hence on the CCSN explosion energy $E_{\rm expl}$. CCSNe with low to medium $E_{\rm expl}$ can produce most of the range $0 \lesssim \log\epsilon({\rm Ba}) \lesssim 2.5$ observed in CEMP-s and CEMP-r/s stars. For example, $\log\epsilon({\rm Ba}) \sim 2$ can be obtained from $25\,{\rm M}_\odot$ models with [Fe/H] ~ -3 and $10^{-5}\,{\rm M}_\odot \lesssim M_{\rm p} \lesssim 10^{-3}\,{\rm M}_\odot$ for a dilution mass of $\sim 10^2\,{\rm M}_\odot$ corresponding to low $E_{\rm expl}$. CCSNe with higher $E_{\rm expl}$ can explain CEMP-s, CEMP-no, or even normal non-CEMP stars, depending on the details of mixing among the heavy elements, C, and Fe, all of which are produced in distinct regions. In general, CCSNe with low to medium $E_{\rm expl}$ would eject most of the material and hence the heavy elements in the He shell, along with a larger fraction of C than Fe in the inner part. Such CCSNe would account for CEMP stars with [C/Fe] > 0.7 and [Ba/Fe] from < 0 (CEMP-no) to > 1 (CEMP-s), as well as VMP stars with $0 <$ [Ba/Fe] < 1. The characteristic [Ba/Eu] for CEMP-s (> 0.5) and CEMP-r/s ($\lesssim 0.5$) stars can also be obtained for different duration Δ of neutron capture in the pre-CCSN star. The above framework for relating

our proposed neutron-capture site in early massive stars to the diversity of VMP stars is illustrated in Fig. 12.

The four VMP stars shown in Fig. 9 are difficult to explain by the existing paradigm. CS 30301-015 (Aoki et al. 2002) (Fig. 9a) appears to be a single CEMP-*s* star (Hansen et al. 2016b) in contradiction to the prevalent explanation of CEMP-*s* stars by mass transfer from an AGB companion during binary evolution. CS 22964-161 (Thompson et al. 2008) (Fig. 9b) represents two CEMP-*s* stars orbiting each other with no sign of a white dwarf left behind by a former AGB companion. Unless the evolution of a triple-star system somehow resulted in the ejection of the white dwarf and the formation of a binary system (Donnison & Mikulskis 1992), observations of CS 22964-161 and its current companion are also in conflict with the scenario of surface pollution by mass transfer. In contrast, low-mass CEMP-*s* stars in both single and binary configurations can form naturally from an ISM enriched by a metal-poor CCSN based on our models with $\Delta > 10^6$ s. The same is also true for CEMP-r/s stars based on our models with $\Delta \lesssim 10^6$ s. HE 2258-6358 (Placco et al. 2013) (Fig. 9c) is an example of a CEMP-r/s star in good agreement with our model. Finally, CS 29493-090 (Spite et al. 2014) (Fig. 9d) is a CEMP star ([C/Fe] = 0.73) that does not show any sign of binarity and has an *s*-like pattern with a low enrichment of $\log\epsilon$(Ba) = −0.49. Its intermediate value of [Ba/Fe] = 0.43 excludes it from being classified as either a CEMP-no or CEMP-*s* star. This and other similar stars reported in Spite et al. (2014) are difficult to explain by the existing paradigm. Such stars with $0 <$ [Ba/Fe] < 1, however, are a natural consequence of neutron-capture nucleosynthesis by our proposed site followed by a CCSN with low to medium explosion energy as discussed above.

4.3. C *Abundances in CEMP Stars*

The majority of CEMP-no stars have lower C enrichment with a mean abundance of $\log\epsilon(\mathrm{C}) \sim 6.3 \pm 0.5$ compared to the majority of CEMP-*s* and CEMP-r/s stars with a mean abundance of $\log\epsilon(\mathrm{C}) \sim 8.0 \pm 0.4$ (Spite et al. 2013; Bonifacio et al. 2015; Hansen et al. 2015; Yoon et al. 2016). This difference in C enrichment is consistent with the framework based on our proposed neutron-capture site as illustrated in Fig. 12, where CCSN sources for CEMP-no stars are more energetic than those for CEMP-*s* and CEMP-r/s stars. More energetic CCSNe would have a larger mass of ISM to dilute their ejecta, thereby causing the lower C enrichment for CEMP-no stars. For example, a 25 $\mathrm{M}_\odot$ star produces 0.3 $\mathrm{M}_\odot$ of C in total, which must be diluted by $\sim 1.6 \times 10^4$ $\mathrm{M}_\odot$ of ISM to give $\log\epsilon(\mathrm{C}) \sim 6.3$. This dilution mass is expected for a CCSN with an explosion energy of $\sim 10^{51}$ ergs. Such a source with $[Z] \lesssim -2$ would also result in $\log\epsilon(\mathrm{Ba}) \lesssim 0$, similar to the Ba enrichment observed in many CEMP-no stars. On the other hand, a low dilution of $\lesssim 1{,}000$ $\mathrm{M}_\odot$ as required to explain CEMP-*s* and CEMP-r/s stars would correspond to a faint CCSN with substantial fallback of the inner material including the C and O shells. The presence of ~ 0.1 $\mathrm{M}_\odot$ of C in the He shell, however, can still result in $\log\epsilon(\mathrm{C}) \sim 7$–$8$ for a dilution mass of ~ 100–$1{,}000$ $\mathrm{M}_\odot$. This estimate is consistent with the C enrichment found in CEMP-*s* and CEMP-r/s stars. Ejection of additional C and O from the inner C and O shells would depend on the details of mixing.

5. SUMMARY AND OUTLOOK

We have proposed a new neutron-capture site associated with proton ingestion in convective He shells of early stars of $\sim$ 20–30 $\mathrm{M}_\odot$. The nucleosynthesis by this site has similar characteristics to the *i*-process that has been studied in connection with proton ingestion in AGB stars. We find that although an r/s-like pattern typically results from the *i*-process with high exposure at high neutron densities, this pattern can be easily and quickly changed to an *s*-like pattern by subsequent low exposure at low neutron densities. Thus, attaining *i*-process neutron densities does not necessarily result in r/s-like patterns. To retain such patterns requires no subsequent low exposure at low neutron densities. This requirement can be fulfilled by the onset of core collapse of the massive star associated with our proposed site. On the other hand, it is difficult to avoid some low exposure at low neutron densities following the *i*-process in AGB stars. How this exposure may modify the yield pattern of the *i*-process remains to be investigated.

As discussed in §4, our proposed site can potentially account for both single and binary CEMP stars with a wide range of patterns and absolute abundances of heavy elements. Consequently, at least some CEMP-*s* and CEMP-r/s stars may have originated directly from the ISM in the same way as CEMP-no stars (see Fig. 12). CEMP-*s* and CEMP-r/s stars require CCSN sources with low energy explosions to ensure low dilution of nucleosynthesis products from the proposed site, whereas CEMP-no stars can have sources with medium energy explosions. This scenario is possible because the heavy elements synthesized in the He shell can be ejected even by weak explosions.

In the current paradigm, only CEMP-no stars are thought to represent the composition of the early ISM enriched by the very first massive stars. The widely accepted scenario for the formation of a CEMP-*s* star is

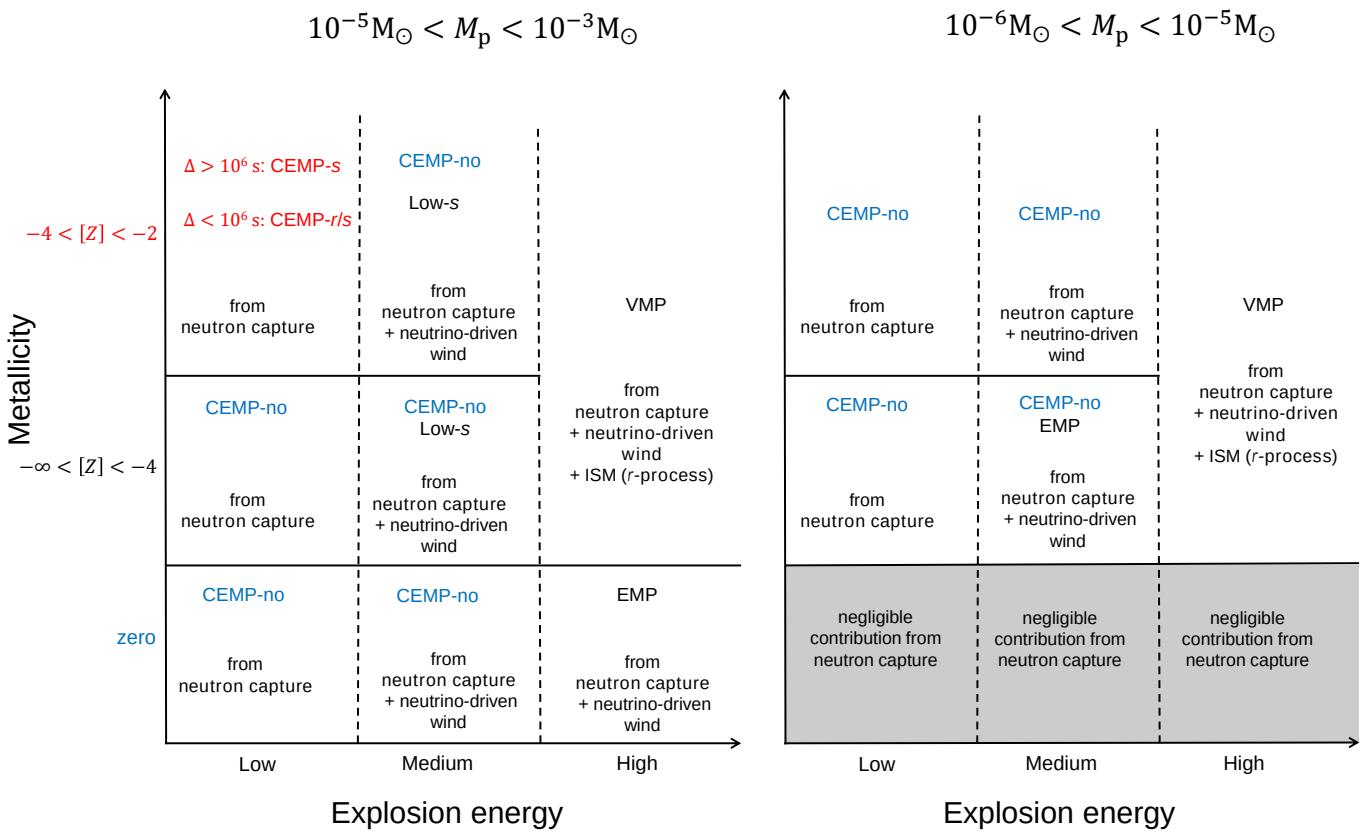

Figure 12. Schematic framework for relating the proposed neutron-capture site in early massive stars to various classes of VMP stars. Three sources for heavy elements are indicated: neutron capture at the proposed site, neutrino-driven winds from the associated CCSN, and *r*-process enrichment in the ISM. VMP and EMP stand for very ([Fe/H] $\lesssim -2$) and extremely ([Fe/H] $\lesssim -3$) metal-poor stars, respectively. Low-*s* stands for stars with *s*-like patterns but low abundances of heavy elements.

surface pollution through binary mass transfer from a heavier companion during its AGB phase. In this scenario, the CEMP-*s* star should be observed today to orbit around the white dwarf left behind by the former AGB companion, which is consistent with the high binary frequency of $\sim 80\,\%$ for such stars as compared to $\sim 17\,\%$ for CEMP-no stars (Hansen et al. 2016a,b). In addition, this scenario can explain both the abundance pattern and the large enhancement of heavy elements and C for most CEMP-*s* stars. The $\sim 20\,\%$ of CEMP-*s* stars that appear to be single, however, require that their surface abundances reflect the composition of the ISM from which they formed instead of pollution by binary mass transfer. Enrichment of the ISM by CCSNe associated with our proposed site would account for these single CEMP-*s* stars (see Fig. 12).

We note that spinstars may also be sources for single CEMP-*s* stars (Choplin et al. 2017). In fact, this model can explain the four apparent single CEMP-*s* stars found by Hansen et al. (2016b) reasonably well. Its potential weakness is that it can only account for very little Pb. Incidentally, three of the above four stars do not have Pb measurement yet, and most CEMP-*s* stars with Pb measurement tend to have high Pb abundances. Future measurement of Pb abundances in single CEMP-*s* stars would help clarify whether spinstars can also be sources for such stars.

Because stars in both single and binary configurations can form from the ISM, some CEMP-*s* stars in binaries could have formed from the same ISM that gave birth to single low-mass CEMP-*s* stars. If a binary of two low-mass stars was formed, this scenario would explain binaries of two CEMP-*s* stars like CS 22964-161 (Thompson et al. 2008). On the other hand, if a low-mass star was formed with a companion of $\sim$ 1–8 $\mathrm{M}_\odot$, the companion during its AGB phase would have polluted the surface of the low-mass star and subsequently left behind a white dwarf. This scenario is similar to the current paradigm for CEMP-*s* stars, except that the low-mass star was born with heavy elements and its birth compo-

sition was later superposed on its surface with the new C and s-process products from its AGB companion. This interesting scenario may lead to some special features in the heavy-element pattern and should be explored by further studies.

Although the origin of CEMP-r/s stars is still uncertain, all the previously proposed scenarios are based on surface pollution by binary mass transfer from a companion of low to intermediate mass, similarly to CEMP-s stars. The binary fraction of CEMP-r/s stars is unclear at present due to limited data. Determination of this fraction by future surveys is particularly important in evaluating our proposed neutron-capture site as an explanation for CEMP-r/s stars. Our framework based on this site would predict that single CEMP-r/s stars should occur with a frequency comparable to single CEMP-s stars. In addition, there should be "low-s" stars with similar patterns of heavy elements to CEMP-s and CEMP-r/s stars but with low enrichment of these elements ($0 <$ [Ba/Fe] < 1). CS 29493-090 (Spite et al. 2014) is such an example. In general, the low-s stars should have similar C enhancement to CEMP-no stars and be observed both as single stars and with a lower binary frequency than CEMP-s stars.

At [Fe/H] $\gtrsim -3.5$, the ISM could have been polluted by r-process sources such as neutron star mergers and jet-driven CCSNe. If neutron-capture nucleosynthesis by our proposed site in massive stars of those times was followed by CCSNe with high explosion energies of $\gtrsim 10^{51}$ ergs, heavy elements produced with an s-like or r/s-like pattern would be mixed broadly with the r-process products in the ISM. Stars formed from such an ISM would have patterns with clear deviation from the r-process kind. Indeed, VMP stars with [Fe/H] as low as ~ -3.5 were observed to have non-r-process values of [Ba/Eu] and [La/Eu] (Simmerer et al. 2004; Suda et al. 2008). This observation is consistent with the above scenario, but difficult to explain otherwise because no pervasive s-process enrichment of the ISM is expected from AGB stars at such early times. We predict that future measurements of detailed heavy-element patterns in single VMP stars will reveal many cases of mixed contributions from the r-process and the neutron-capture nucleosynthesis by our proposed site. We note that HD 94028 with [Fe/H] ≈ -1.6, somewhat outside the range of [Fe/H] $\lesssim -2$ for the VMP stars of concern here, appears to have received neutron-capture elements from multiple sources (Roederer et al. 2016). Whereas we have focused on Sr, Ba, La, Eu, and Pb as specific elements of interest, the element As in this and perhaps other similar stars may have originated from the i-process (Roederer et al. 2016). This important issue and the overall patterns of neutron-capture elements in such stars are outside our scope here but certainly merit further detailed studies.

With the proposed site operating in metal-free and metal-poor stars of ~ 20–$30\,M_\odot$, important constraints may be set on the formation mode for stars of populations III and II. The present study has focused on the heavy elements. In the future, we plan to include both these and lighter elements in the mixing and fallback prescription for CCSN ejecta to make full comparison with observations, thereby probing the allowed mass range of early CCSN sources. We note that other recent studies used the patterns of elements up to the Fe group in CEMP-no stars to constrain the mass range of their metal-free CCSN sources (Placco et al. 2016). How the allowed mass range would be affected by including the heavy elements from our proposed site in such studies remains to be seen.

Several crucial aspects of our proposed neutron-capture site require further investigation. The foremost is accurate 3D modeling of proton ingestion and especially the subsequent mixing in He shells of metal-free and metal-poor massive stars. Neutron production at this site relies on successful transport of the ingested protons to the base of the He shell. This transport can be modelled properly only in 3D. Finally, reliable simulations of the associated CCSNe are also important, because the ejection of various nucleosynthesis products from different layers is crucial in determining the overall yield pattern including both the heavy and lighter elements for comparison with observations.

We thank the anonymous referee for criticisms and suggestions that helped improve the paper. We made extensive use of the SAGA database (Suda et al. 2008). This work was supported in part by the NSFC [11533006 (SJTU)], the US DOE [DE-FG02-87ER40328 (UM)], and the ARC [FT120100363 (Monash)].

Software: KEPLER (Weaver et al. 1978; Rauscher et al. 2003)

REFERENCES

Aoki, W., Ryan, S. G., Norris, J. E., et al. 2002, ApJ, 580, 1149

Arcones, A., & Montes, F. 2011, ApJ, 731, 5

Arcones, A., & Thielemann, F.-K. 2013, J. Phys. G Nucl. Partic., 40, 013201
Bao, Z. Y., Beer, H., Käppeler, F., et al. 2000, Atomic Data and Nuclear Data Tables, 76, 70
Baraffe, I., El Eid, M. F., & Prantzos, N. 1992, A&A, 258, 357
Barbuy, B., Spite, M., Spite, F., et al. 2005, A&A, 429, 1031
Beers, T. C., & Christlieb, N. 2005, ARA&A, 43, 531
Bisterzo, S., Gallino, R., Straniero, O., Cristallo, S., & Käppeler, F. 2012, Mon. Not. R. Astron. Soc., 422, 849
Bonifacio, P., Caffau, E., Spite, M., et al. 2015, A&A, 579, A28
Buchmann, L. 1996, ApJL, 468, L127
Campbell, S. W., Lugaro, M., & Karakas, A. I. 2010, A&A, 522, L6
Caughlan, G. R., & Fowler, W. A. 1988, At. Data Nucl. Data Tables, 40, 283
Choplin, A., Hirschi, R., Meynet, G., & Ekström, S. 2017, A&A, 607, L3
Clarkson, O., Herwig, F., & Pignatari, M. 2018, MNRAS, 474, L37
Cohen, J. G., Christlieb, N., Qian, Y.-Z., & Wasserburg, G. J. 2003, ApJ, 588, 1082
Cowan, J. J., & Rose, W. K. 1977, ApJ, 212, 149
Dardelet, L., Ritter, C., Prado, P., et al. 2014, in XIII Nuclei in the Cosmos (NIC XIII), 145
Denissenkov, P. A., Herwig, F., Battino, U., et al. 2017, ApJL, 834, L10
Donnison, J. R., & Mikulskis, D. F. 1992, MNRAS, 254, 21
Eichler, D., Livio, M., Piran, T., & Schramm, D. N. 1989, Nature, 340, 126
Fowler, W. A., Caughlan, G. R., & Zimmerman, B. A. 1975, ARA&A, 13, 69
Freiburghaus, C., Rosswog, S., & Thielemann, F.-K. 1999, ApJL, 525, L121
Frischknecht, U., Hirschi, R., Pignatari, M., et al. 2016, MNRAS, 456, 1803
Fujimoto, M. Y., Ikeda, Y., & Iben, Jr., I. 2000, ApJL, 529, L25
Hampel, M., Stancliffe, R. J., Lugaro, M., & Meyer, B. S. 2016, ApJ, 831, 171
Hansen, T., Hansen, C. J., Christlieb, N., et al. 2015, ApJ, 807, 173
Hansen, T. T., Andersen, J., Nordström, B., et al. 2016a, A&A, 586, A160
—. 2016b, A&A, 588, A3
Harris, M. J., Fowler, W. A., Caughlan, G. R., & Zimmerman, B. A. 1983, ARA&A, 21, 165
Heger, A., & Woosley, S. E. 2010, ApJ, 724, 341
Herwig, F. 2000, A&A, 360, 952
Herwig, F., Pignatari, M., Woodward, P. R., et al. 2011, ApJ, 727, 89
Herwig, F., Woodward, P. R., Lin, P.-H., Knox, M., & Fryer, C. 2014, ApJL, 792, L3
Hoffman, R. D., Woosley, S. E., & Weaver, T. A. 2001, ApJ, 549, 1085
Jones, S., Ritter, C., Herwig, F., et al. 2016, Mon. Not. R. Astron. Soc., arXiv:1510.07417
Jonsell, K., Barklem, P. S., Gustafsson, B., et al. 2006, A&A, 451, 651
Käppeler, F., Gallino, R., Bisterzo, S., & Aoki, W. 2011, Rev. Mod. Phys., 83, 157
Keller, S. C., Bessell, M. S., Frebel, A., et al. 2014, Nature, 506, 463
Landre, V., Prantzos, N., Aguer, P., et al. 1990, A&A, 240, 85
Lattimer, J. M., & Schramm, D. N. 1974, ApJL, 192, L145
Limongi, M., & Chieffi, A. 2012, ApJS, 199, 38
Lucatello, S., Tsangarides, S., Beers, T. C., et al. 2005, ApJ, 625, 825
Lugaro, M., Karakas, A. I., Stancliffe, R. J., & Rijs, C. 2012, ApJ, 747, 2
Meakin, C. A., & Arnett, D. 2007, ApJ, 667, 448
Meynet, G., Ekström, S., & Maeder, A. 2006, A&A, 447, 623
Nomoto, K., Tominaga, N., Umeda, H., et al. 2005, Nuc. Phys. A, 758, 263
Paxton, B., Bildsten, L., Dotter, A., et al. 2011, ApJS, 192, 3
Pignatari, M., Gallino, R., Meynet, G., et al. 2008, ApJL, 687, L95
Placco, V. M., Frebel, A., Beers, T. C., et al. 2013, ApJ, 770, 104
—. 2016, ApJ, 833, 21
Rauscher, T., Applegate, J. H., Cowan, J. J., Thielemann, F.-K., & Wiescher, M. 1994, ApJ, 429, 499
Rauscher, T., Heger, A., Hoffman, R. D., & Woosley, S. E. 2002, ApJ, 576, 323
—. 2003, Nucl. Phys. A, 718, 463
Rauscher, T., Thielemann, F.-K., Görres, J., & Wiescher, M. 2000, Nuclear Physics A, 675, 695
Roberts, L. F., Woosley, S. E., & Hoffman, R. D. 2010, ApJ, 722, 954
Roederer, I. U. 2013, AJ, 145, 26
Roederer, I. U., Cowan, J. J., Preston, G. W., et al. 2014a, Mon. Not. R. Astron. Soc., 445, 2970
Roederer, I. U., Karakas, A. I., Pignatari, M., & Herwig, F. 2016, ApJ, 821, 37

Roederer, I. U., Preston, G. W., Thompson, I. B., et al. 2014b, Astron. J., 147, 136

Simmerer, J., Sneden, C., Cowan, J. J., et al. 2004, ApJ, 617, 1091

Spite, M., Caffau, E., Bonifacio, P., et al. 2013, A&A, 552, A107

Spite, M., Spite, F., Bonifacio, P., et al. 2014, A&A, 571, A40

Stancliffe, R. J., Dearborn, D. S. P., Lattanzio, J. C., Heap, S. A., & Campbell, S. W. 2011, ApJ, 742, 121

Suda, T., Katsuta, Y., Yamada, S., et al. 2008, Publ. Astron. Soc. Jpn., 60, 1159

Sukhbold, T., & Woosley, S. E. 2014, ApJ, 783, 10

Thielemann, F.-K., A. M., & Truran, J. 1987, in Advances in Nuclear Astrophysics, ed. E. Vangioni-Flam (Gif sur Yvette: Editions Frontire), 529

Thielemann, F.-K., e. a. 1995, Reaction Rate Library REACLIB

Thompson, I. B., Ivans, I. I., Bisterzo, S., et al. 2008, ApJ, 677, 556

Tominaga, N., Iwamoto, N., & Nomoto, K. 2014, ApJ, 785, 98

Umeda, H., & Nomoto, K. 2005, ApJ, 619, 427

Weaver, T. A., Zimmerman, G. B., & Woosley, S. E. 1978, ApJ, 225, 1021

Wiescher, M., Gorres, J., Thielemann, F.-K., & Ritter, H. 1986, A&A, 160, 56

Winteler, C., Käppeli, R., Perego, A., et al. 2012, ApJL, 750, L22

Wrean, P. R., Brune, C. R., & Kavanagh, R. W. 1994, PhRvC, 49, 1205

Yoon, J., Beers, T. C., Placco, V. M., et al. 2016, ApJ, 833, 20

Table 1. References for key reaction rates. BAAL: Bao et al. (2000), W94: Wrean et al. (1994), FCZ2: Fowler et al. (1975), HFCZ: Harris et al. (1983), BU96: Buchmann (1996), CF88: Caughlan & Fowler (1988), WIES: Wiescher et al. (1986), RATH: Rauscher et al. (2000), FKTH: Thielemann & Truran (1987); Thielemann (1995), RA94: Rauscher et al. (1994), LA90: Landre et al. (1990), HW01: Hoffman et al. (2001).

^{A}Z	(n,γ)	(n,p)	(n,α)	(p,n)	(p,γ)	(p,α)	(α,p)	(α,n)	(α,γ)
^{12}C	BAAL		W94		FCZ2		HFCZ	HFCZ	BU96
^{13}C	RA94			FCZ2	CF88			FCZ2	
^{13}N	WIES	FCZ2	CF88		KL93		HFCZ		
^{14}N	WIES	CF88	CF88	FCZ2	CF88	CF88	HW01	CF88	FCZ2
^{16}O	BAAL		FCZ2		FCZ2	HFCZ	HFCZ	RATH	CF88
^{17}O	RA94			FKTH	LA90	HW01		FCZ2	FCZ2

Table 2. Pre-CCSN yields (in $M_\odot$) of Sr, Ba, La, Eu, and Pb for 25 $M_\odot$ stars with metallicity $[Z]$ and ingested proton mass M_p. Ingestion occurs only once at central C depletion unless noted otherwise. Here $X(Y) \equiv X \times 10^Y$.

Model	Sr	Ba	La	Eu	Pb
$[Z] = -\infty$, $M_p = 10^{-3}\,M_\odot$	9.85(-14)	1.16(-14)	3.21(-16)	2.93(-17)	6.74(-17)
$[Z] = -\infty$, 3 pulses of $M_p = 10^{-4}\,M_\odot$ every 10^6 s	4.65(-11)	1.44(-10)	6.40(-12)	2.96(-13)	3.09(-10)
$[Z] = -\infty$, 2 pulses of $M_p = 10^{-4}\,M_\odot$ every 10^6 s	1.69(-11)	5.91(-11)	2.72(-12)	1.26(-13)	1.09(-10)
$[Z] = -\infty$, $M_p = 10^{-4}\,M_\odot$	6.42(-12)	1.85(-11)	8.17(-13)	3.37(-14)	1.67(-11)
$[Z] = -\infty$, $M_p = 5 \times 10^{-5}\,M_\odot$	5.12(-12)	1.39(-11)	6.08(-13)	2.35(-14)	1.02(-11)
$[Z] = -\infty$, $M_p = 10^{-5}\,M_\odot$	5.80(-13)	2.70(-13)	8.76(-15)	1.96(-16)	1.45(-14)
$[Z] = -\infty$, $M_p = 10^{-6}\,M_\odot$	1.82(-14)	2.63(-15)	1.71(-16)	2.51(-17)	0.00
$[Z] = -5$, $M_p = 10^{-3}\,M_\odot$	2.41(-9)	2.15(-9)	8.87(-11)	4.01(-12)	5.92(-10)
$[Z] = -5$, $M_p = 10^{-4}\,M_\odot$	9.21(-10)	4.71(-9)	2.66(-10)	1.67(-11)	2.09(-8)
$[Z] = -5$, $M_p = 10^{-5}\,M_\odot$	2.28(-9)	4.55(-9)	1.84(-10)	7.80(-12)	1.31(-9)
$[Z] = -5$, $M_p = 10^{-6}\,M_\odot$	2.88(-9)	7.78(-10)	3.70(-11)	1.17(-12)	3.70(-11)
$[Z] = -4$, $M_p = 10^{-3}\,M_\odot$	8.90(-9)	5.32(-8)	2.76(-9)	1.57(-10)	1.51(-7)
$[Z] = -4$, $M_p = 10^{-4}\,M_\odot$	9.84(-9)	5.56(-8)	3.07(-9)	1.46(-10)	1.64(-7)
$[Z] = -4$, $M_p = 10^{-5}\,M_\odot$	1.84(-8)	1.10(-8)	3.90(-10)	6.67(-12)	4.09(-10)
$[Z] = -4$, $M_p = 10^{-6}\,M_\odot$	2.81(-10)	1.66(-14)	1.59(-16)	2.41(-18)	0.00
$[Z] = -3$, $M_p = 10^{-3}\,M_\odot$	8.74(-8)	5.22(-7)	2.66(-8)	1.32(-9)	1.38(-6)
$[Z] = -3$, $M_p = 10^{-4}\,M_\odot$	9.49(-8)	5.44(-7)	3.03(-8)	1.26(-9)	1.63(-6)
$[Z] = -3$, $M_p = 5 \times 10^{-5}\,M_\odot$	1.21(-7)	5.73(-7)	3.12(-8)	1.25(-9)	9.53(-7)
$[Z] = -3$, $M_p = 10^{-5}\,M_\odot$	1.86(-7)	1.42(-7)	5.70(-9)	1.52(-10)	8.60(-9)
$[Z] = -3$, $M_p = 5 \times 10^{-6}\,M_\odot$	1.03(-7)	1.19(-8)	3.49(-10)	6.85(-12)	5.38(-11)
$[Z] = -3$, $M_p = 10^{-6}\,M_\odot$	2.23(-9)	2.24(-13)	1.66(-15)	3.71(-18)	0.00
$[Z] = -2$, $M_p = 10^{-3}\,M_\odot$	8.37(-7)	4.92(-6)	2.41(-7)	1.43(-8)	1.26(-5)
$[Z] = -2$, $M_p = 10^{-4}\,M_\odot$	1.03(-6)	4.73(-6)	2.23(-7)	1.37(-8)	7.47(-6)
$[Z] = -2$, $M_p = 10^{-5}\,M_\odot$	2.15(-7)	2.84(-9)	3.34(-11)	3.78(-13)	6.55(-13)
$[Z] = -2$, $M_p = 10^{-6}\,M_\odot$	3.02(-12)	0.00	0.00	0.00	0.00
$[Z] = -1$, $M_p = 10^{-3}\,M_\odot$	1.19(-5)	1.76(-5)	6.06(-7)	2.11(-8)	3.80(-6)
$[Z] = -1$, $M_p = 10^{-4}\,M_\odot$	5.23(-5)	2.66(-7)	7.70(-9)	6.34(-10)	5.15(-8)
$[Z] = -1$, $M_p = 5 \times 10^{-5}\,M_\odot$	8.39(-7)	5.86(-8)	4.77(-9)	5.93(-10)	4.94(-8)
$[Z] = -1$, $M_p = 10^{-5}\,M_\odot$	3.86(-7)	5.79(-8)	4.79(-9)	5.93(-10)	4.63(-8)
$[Z] = -1$, without proton ingestion	3.87(-7)	5.69(-8)	4.70(-9)	5.94(-10)	4.51(-8)

Table 3. Post-CCSN yields (in $M_\odot$) of Sr, Ba, La, Eu, and Pb for $25\,M_\odot$ stars with metallicity $[Z]$, ingested proton mass M_p, and explosion energy E_{expl} (Models 1–6) used for comparison with VMP stars. Here $X(Y) \equiv X \times 10^Y$, and Cdep (Odep) denotes central C (O) depletion.

Model	Sr	Ba	La	Eu	Pb
Model 1: $[Z] = -3, M_p = 5 \times 10^{-5}\,M_\odot$ at Cdep, $E_{expl} = 10^{50}$ ergs	1.21(-7)	5.75(-7)	3.29(-8)	1.51(-9)	9.58(-7)
Model 2: $[Z] = -3, M_p = 10^{-4}\,M_\odot$ at Cdep, $E_{expl} = 10^{50}$ ergs	9.48(-8)	5.45(-7)	3.16(-8)	1.50(-9)	1.64(-6)
Model 3: $[Z] = -3, M_p = 10^{-4}\,M_\odot$ at Odep, $E_{expl} = 10^{50}$ ergs	8.52(-8)	4.12(-7)	2.52(-8)	2.69(-9)	9.93(-7)
Model 4: $[Z] = -4, M_p = 10^{-4}\,M_\odot$ at Odep, $E_{expl} = 3 \times 10^{50}$ ergs	8.57(-9)	4.15(-8)	2.56(-9)	2.82(-10)	1.03(-7)
Model 5: $[Z] = -2.5$, 2 pulses of $M_p = 5 \times 10^{-4}\,M_\odot$ at Cdep and 10^6 s later, $E_{expl} = 10^{50}$ ergs	1.84(-7)	1.71(-6)	1.09(-7)	7.50(-9)	7.48(-6)
Model 6: $[Z] = -2.5$, 2 pulses of $M_p = 5 \times 10^{-4}\,M_\odot$ at Cdep and Odep, $E_{expl} = 10^{50}$ ergs	1.91(-7)	1.35(-6)	9.50(-8)	1.19(-8)	6.06(-6)